MODIFIED SHALLOW WATER EQUATIONS FOR SIGNIFICANTLY VARYING BOTTOMS

DENYS DUTYKH* AND DIDIER CLAMOND

Abstract. In the present study we propose an modified version of the nonlinear shallow water (Saint-Venant) equations for the case when the bottom undergoes some significant variations in space and *time*. The model is derived from a variational principle by choosing the appropriate shallow water ansatz and imposing some constraints. Our derivation procedure does not explicitly involve any small parameter and is straightforward. The novel system is a non-dispersive, *and* non-hydrostatic extension of the classical Saint-Venant equations. We also propose a finite volume discretization of the obtained hyperbolic system. Several test-cases are presented to highlight the added value of the new model. Some implications to tsunami wave modelling are also discussed.

Contents

Key words and phrases. Shallow water; Saint-Venant equations; finite volumes; UNO scheme.
* Corresponding author.

1. Introduction

The celebrated classical nonlinear shallow water or Saint-Venant equations were derived for the first time in 1871 by A.J.C. de Saint-Venant [17], an engineer working at *École Nationale des Ponts et Chaussées* in France. Currently these equations are widely used in practice and the literature counts many thousands of publications devoted to the applications, validations and numerical solutions of these equations [2, 34, 35, 38, 75, 88].

Some important attempts have been also made to improve this model from physical point of view. The main attention was payed to various dispersive extensions of shallow water equations. The inclusion of dispersive effects resulted in a big family of the so-called Boussinesq-type equations [21, 26, 32, 54, 57, 58, 60, 63]. Many other families of dispersive wave equations have been proposed as well [14, 18, 20, 42, 56, 67, 81].

However, the interaction of the waves with mild or tough bottoms has always attracted the particular attention of researchers [58, 6, 13, 33]. There are a few studies which attempt to include the bottom curvature effect into the classical Saint-Venant [17, 72] or Savage-Hutter[1] [66, 41, 86] equations. One of the first studies in this direction is perhaps due to Dressler [22]. Much later, this research was pursued almost in the same time by Keller, Bouchut and their collaborators [49, 11]. We note that all these authors used some variants of the asymptotic expansion method. The present study is a further attempt to improve the classical Saint-Venant equations by including a better representation of the bottom shape. Moreover, as a derivation procedure we choose a variational approach based on the relaxed Lagrangian principle [16]. The derivation presented below was already communicated by the same authors in a short note announcing the main results [25]. In this study we investigate deeper the properties of the proposed system along with its solutions through analytical and numerical methods. The obtained results may improve the modeling of various types of shallow water flows such as open channel hydraulics [15], atmospheric and oceanic flows [61], waves in coastal areas [9, 5, 30, 32], and even dense snow avalanches [66, 47, 86].

The present article is organized as follows. After some introductory remarks, the paper begins with the derivation and discussion of some properties of the modified Saint-Venant (mSV) equations in Section 2. Then, we investigate the hyperbolic structure and present a finite volume scheme in Section 3. Several numerical results are shown in Section 4. Finally, some main conclusions are outlined in the last Section 5.

2. Mathematical model

Consider an ideal incompressible fluid of constant density ρ. The horizontal independent variables are denoted by $\boldsymbol{x} = (x_1, x_2)$ and the upward vertical one by y. The origin of the Cartesian coordinate system is chosen such that the surface $y = 0$ corresponds to the still water level. The fluid is bounded below by the bottom at $y = -d(\boldsymbol{x}, t)$ and above by the free surface at $y = \eta(\boldsymbol{x}, t)$. Usually, we assume that the total depth $h(\boldsymbol{x}, t) \equiv d(\boldsymbol{x}, t) + \eta(\boldsymbol{x}, t)$

[1] The Savage–Hutter equations are usually posed on inclined planes and they are used to model various gravity driven currents, such as snow avalanches [4].

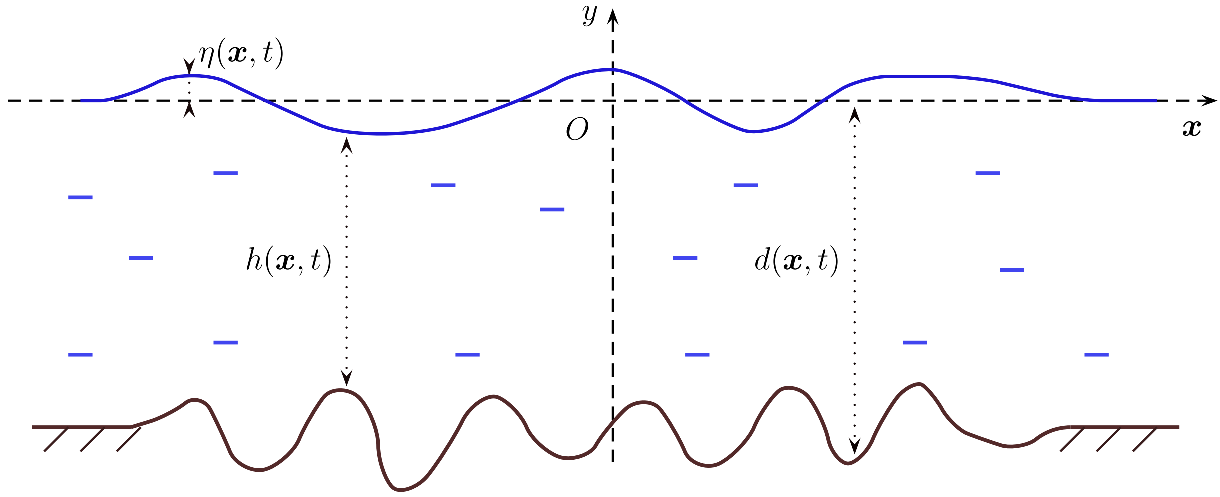

FIGURE 1. Definition sketch.

remains positive $h(\boldsymbol{x}, t) \geqslant h_0 > 0$ at all times $t \in [0, T]$. The sketch of the physical domain $\Omega \times [-d, \eta]$, $\Omega \subseteq \mathbb{R}^2$ is shown on Figure 1.

Traditionally in water wave modelling the assumption of flow irrotationality is also adopted. Under these constitutive hypotheses, the governing equations of the classical water wave problem are [52, 73, 55, 84, 48]:

$$\boldsymbol{\nabla}^2\phi + \partial_y^2\phi = 0, \qquad (\boldsymbol{x}, y) \in \Omega \times [-d, \eta], \tag{2.1}$$
$$\partial_t\eta + (\boldsymbol{\nabla}\phi)\cdot(\boldsymbol{\nabla}\eta) - \partial_y\phi = 0, \qquad y = \eta(\boldsymbol{x}, t), \tag{2.2}$$
$$\partial_t\phi + \tfrac{1}{2}|\boldsymbol{\nabla}\phi|^2 + \tfrac{1}{2}(\partial_y\phi)^2 + g\eta = 0, \qquad y = \eta(\boldsymbol{x}, t), \tag{2.3}$$
$$\partial_t d + (\boldsymbol{\nabla}d)\cdot(\boldsymbol{\nabla}\phi) + \partial_y\phi = 0, \qquad y = -d(\boldsymbol{x}, t), \tag{2.4}$$

where ϕ is the velocity potential (by definition, $\boldsymbol{u} = \boldsymbol{\nabla}\phi$ and $v = \partial_y\phi$), $g > 0$ is the acceleration due to gravity and $\boldsymbol{\nabla} = (\partial_{x_1}, \partial_{x_2})$ denotes the gradient operator in horizontal Cartesian coordinates.

The assumptions of fluid incompressibility and flow irrotationality lead to the Laplace equation (2.1) for the velocity potential $\phi(\boldsymbol{x}, y, t)$. The main difficulty of the water wave problem lies on the boundary conditions. Equations (2.2) and (2.4) express the free-surface kinematic condition and bottom impermeability, respectively, while the dynamic condition (2.3) expresses the free surface isobarity.

It is well-known that the water wave problem (2.1) – (2.4) possesses several variational structures [64, 83, 53, 87, 12]. Recently, we proposed a relaxed Lagrangian variational principle which allows much more freedom in constructing approximations compared to

the classical formulations. Namely, the water wave equations can be obtained as Euler–Lagrange equations of the functional $\iiint \mathscr{L}\,\mathrm{d}^2\boldsymbol{x}\,\mathrm{d}t$ involving the Lagrangian density [16]:

$$\mathscr{L} \;=\; (\partial_t\eta + \tilde{\boldsymbol{\mu}}\boldsymbol{\cdot}\boldsymbol{\nabla}\eta - \tilde{\nu})\,\tilde{\phi} \;+\; (\partial_t d + \check{\boldsymbol{\mu}}\boldsymbol{\cdot}\boldsymbol{\nabla} d + \check{\nu})\,\check{\phi} \;-\; \tfrac{1}{2}\,g\,\eta^2 \\ +\; \int_{-d}^{\eta} \big[\,\boldsymbol{\mu}\boldsymbol{\cdot}\boldsymbol{u} - \tfrac{1}{2}\boldsymbol{u}^2 \;+\; \nu v - \tfrac{1}{2}v^2 \;+\; (\boldsymbol{\nabla}\boldsymbol{\cdot}\boldsymbol{\mu} + \partial_y\nu)\,\phi\,\big]\,\mathrm{d}y, \qquad (2.5)$$

where the over 'tildes' and 'wedges' denote, respectively, a quantity traces computed at the free surface $y = \eta(\boldsymbol{x}, t)$ and at the bottom $y = -d(\boldsymbol{x}, t)$ (we shall also denote below with 'bars' the quantities averaged over the water depth); $\{\boldsymbol{u}, v, \boldsymbol{\mu}, \nu\}$ being the horizontal velocity, vertical velocity and associated Lagrange multipliers, respectively. The last two additional variables $\{\boldsymbol{\mu}, \nu\}$ are called the pseudo-velocities. They formally arise as Lagrange multipliers associated to the constraints $\boldsymbol{u} = \boldsymbol{\nabla}\phi$, $v = \phi_y$. However, once these variables are introduced, the ansatz can be chosen regardless their initial definition. The advantage of the relaxed variational principle (2.5) consists in the extra freedom for constructing approximations.

2.1. **Constrained shallow water ansatz.** In order to simplify the full water wave problem, we choose some approximate but physically relevant representations of all dependent variables. In this study, we choose a simple shallow water ansatz, which is a velocity field and velocity potential independent of the vertical coordinate y such that

$$\phi \;\approx\; \bar{\phi}(\boldsymbol{x}, t), \qquad \boldsymbol{u} \;=\; \boldsymbol{\mu} \;\approx\; \bar{\boldsymbol{u}}(\boldsymbol{x}, t), \qquad v \;=\; \nu \;\approx\; \check{v}(\boldsymbol{x}, t), \qquad (2.6)$$

where $\check{v}(\boldsymbol{x}, t)$ is the vertical velocity at the bottom. In this ansatz, we take for simplicity the pseudo-velocities to be equal to the velocity field $\boldsymbol{u} = \boldsymbol{\mu}$, $v = \nu$. However, in other situations they can differ (see [16] for more examples). The Lagrangian density (2.5) becomes:

$$\mathscr{L} \;=\; (\partial_t h \;+\; \bar{\boldsymbol{u}}\boldsymbol{\cdot}\boldsymbol{\nabla} h \;+\; h\boldsymbol{\nabla}\boldsymbol{\cdot}\bar{\boldsymbol{u}})\,\bar{\phi} \;-\; \tfrac{1}{2}\,g\,\eta^2 \;+\; \tfrac{1}{2}\,h\,(\bar{\boldsymbol{u}}^2 + \check{v}^2), \qquad (2.7)$$

where we make appear the total water depth $h = \eta + d$.

Remark 1. *Note that for ansatz (2.6) the horizontal vorticity $\boldsymbol{\omega}$ and the vertical one ζ are given by:*

$$\boldsymbol{\omega} = \Big(\partial_{x_2}\check{v}\,,\, -\partial_{x_1}\check{v}\Big), \qquad \zeta = \partial_{x_1}\bar{u}_2 - \partial_{x_2}\bar{u}_1.$$

Consequently the flow is not exactly irrotational in general. It will be confirmed below one more time when we establish the connection between $\bar{\boldsymbol{u}}$ and $\boldsymbol{\nabla}\bar{\phi}$.

Now we are going to impose one constraint by choosing a particular representation of the fluid vertical velocity $\check{v}(\boldsymbol{x}, t)$ at the bottom. Namely, we require fluid particles to follow the bottom profile:

$$\check{v} \;=\; -\partial_t\, d \;-\; \bar{\boldsymbol{u}}\boldsymbol{\cdot}\boldsymbol{\nabla} d. \qquad (2.8)$$

The last identity can be also seen as the bottom impermeabiliy condition within ansatz (2.6). After substituting relation (2.8) into Lagrangian density (2.7), the minimization

procedure yields:

$$\delta\bar{\phi}: \quad 0 \;=\; \partial_t\, h \;+\; \boldsymbol{\nabla}\boldsymbol{\cdot}[\, h\,\bar{\boldsymbol{u}}\,], \tag{2.9}$$

$$\delta\bar{\boldsymbol{u}}: \quad \boldsymbol{0} \;=\; \bar{\boldsymbol{u}} \;-\; \boldsymbol{\nabla}\bar{\phi} \;-\; \check{v}\,\boldsymbol{\nabla} d, \tag{2.10}$$

$$\delta\eta: \quad 0 \;=\; \partial_t\,\bar{\phi} \;+\; g\,\eta \;+\; \bar{\boldsymbol{u}}\boldsymbol{\cdot}\boldsymbol{\nabla}\bar{\phi} \;-\; \tfrac{1}{2}\,(\bar{\boldsymbol{u}}^2+\check{v}^2). \tag{2.11}$$

Taking the gradient of (2.11) and eliminating of $\bar{\phi}$ from (2.10) gives us this system of governing equations:

$$\partial_t\, h \;+\; \boldsymbol{\nabla}\boldsymbol{\cdot}[\, h\,\bar{\boldsymbol{u}}\,] \;=\; 0, \tag{2.12}$$

$$\partial_t\,[\,\bar{\boldsymbol{u}} - \check{v}\,\boldsymbol{\nabla} d\,] \;+\; \boldsymbol{\nabla}\,[\, g\,\eta \;+\; \tfrac{1}{2}\,\bar{\boldsymbol{u}}^2 \;+\; \tfrac{1}{2}\,\check{v}^2 \;+\; \check{v}\,\partial_t d\,] = \;0, \tag{2.13}$$

together with relations:

$$\bar{\boldsymbol{u}} \;=\; \boldsymbol{\nabla}\bar{\phi} \;+\; \check{v}\boldsymbol{\nabla} d, \qquad \check{v} \;=\; -\,\partial_t\, d \;-\; \bar{\boldsymbol{u}}\boldsymbol{\cdot}\boldsymbol{\nabla} d \;=\; -\frac{\partial_t d \;+\; \boldsymbol{\nabla}\bar{\phi}\boldsymbol{\cdot}\boldsymbol{\nabla} d}{1 \;+\; |\boldsymbol{\nabla} d|^2}.$$

Remark 2. *The classical nonlinear shallow water or Saint-Venant equations* [17, 72] *can be recovered by substituting $\check{v} = 0$ into the last system:*

$$\partial_t\, h \;+\; \boldsymbol{\nabla}\boldsymbol{\cdot}[\, h\,\bar{\boldsymbol{u}}\,] \;=\; 0,$$

$$\partial_t\,\bar{\boldsymbol{u}} \;+\; \boldsymbol{\nabla}\,[\, g\,\eta \;+\; \tfrac{1}{2}\,\bar{\boldsymbol{u}}^2] = \;0.$$

The last equation is generally written in the literature into the conservative momentum flux form [19, 65, 34]*:*

$$\partial_t\,[\, h\,\bar{\boldsymbol{u}}\,] \;+\; \boldsymbol{\nabla}\,[\, h\,\bar{\boldsymbol{u}}^2 \;+\; \tfrac{1}{2}\,g\,h^2\,] \;=\; g\,h\,\boldsymbol{\nabla} d.$$

2.2. **Properties of the new model.** From governing equations (2.12), (2.13) one can derive an equation for the horizontal velocity $\bar{\boldsymbol{u}}$ and for the momentum flux $h\bar{\boldsymbol{u}}$:

$$\partial_t\,\bar{\boldsymbol{u}} \;+\; \bar{\boldsymbol{u}}\boldsymbol{\cdot}\boldsymbol{\nabla}\bar{\boldsymbol{u}} \;+\; g\,\boldsymbol{\nabla}\eta \;=\; \gamma\,\boldsymbol{\nabla} d \;+\; \bar{\boldsymbol{u}}\wedge\boldsymbol{\nabla}\check{v}\wedge\boldsymbol{\nabla} d, \tag{2.14}$$

$$\partial_t\,[\, h\,\bar{\boldsymbol{u}}\,] \;+\; \boldsymbol{\nabla}\,[\, h\,\bar{\boldsymbol{u}}^2 \;+\; \tfrac{1}{2}\,g\,h^2\,] \;=\; (g+\gamma)\,h\,\boldsymbol{\nabla} d \;+\; h\bar{\boldsymbol{u}}\wedge\boldsymbol{\nabla}\check{v}\wedge\boldsymbol{\nabla} d, \tag{2.15}$$

where γ is the vertical acceleration at the bottom defined as:

$$\gamma \;\equiv\; \frac{\mathrm{d}\,\check{v}}{\mathrm{d}t} \;=\; \partial_t\,\check{v} \;+\; (\bar{\boldsymbol{u}}\boldsymbol{\cdot}\boldsymbol{\nabla})\check{v}. \tag{2.16}$$

Remark 3. *Note that in equations* (2.14) *and* (2.15) *the last term on the right-hand side cancels out in one horizontal dimension. It can be seen from the following analytical representation which degenerates to zero in one horizontal dimension:*

$$h\,\bar{\boldsymbol{u}}\wedge\boldsymbol{\nabla}\check{v}\wedge\boldsymbol{\nabla} d \;=\; (\boldsymbol{\nabla}\check{v})\,(h\bar{\boldsymbol{u}}\boldsymbol{\cdot}\boldsymbol{\nabla} d) \;-\; (\boldsymbol{\nabla} d)\,(h\bar{\boldsymbol{u}}\boldsymbol{\cdot}\boldsymbol{\nabla}\check{v}).$$

This property has an interesting geometrical interpretation since $h\bar{\boldsymbol{u}}\wedge\boldsymbol{\nabla}\check{v}\wedge\boldsymbol{\nabla} d$ is a horizontal vector orthogonal to $\bar{\boldsymbol{u}}$ and thus vanishing for two-dimensional waves.

One can also derive an equation for the energy flux:

$$\partial_t\left[h\frac{|\bar{\boldsymbol{u}}|^2+\check{v}^2}{2} + g\frac{\eta^2-d^2}{2}\right] \;+\; \boldsymbol{\nabla}\boldsymbol{\cdot}\left[\left(\frac{|\bar{\boldsymbol{u}}|^2+\check{v}^2}{2} + g\eta\right)h\bar{\boldsymbol{u}}\right] \;=\; -(g+\gamma)\,h\,\partial_t d. \tag{2.17}$$

Obviously, the source term on the right-hand side vanishes if the bottom is fixed $d = d(x)$ or, equivalently, $\partial_t d = 0$.

The last conservation law is closely related to the Hamiltonian structure of the mSV equations (2.9)–(2.11). Namely, these equations possess a Hamiltonian structure with canonical variables h and $\bar{\phi}$, i.e.,

$$\frac{\partial h}{\partial t} \;=\; \frac{\delta \mathcal{H}}{\delta \bar{\phi}}, \qquad \frac{\partial \bar{\phi}}{\partial t} \;=\; -\frac{\delta \mathcal{H}}{\delta h},$$

where the Hamiltonian is

$$\mathcal{H} \;=\; \tfrac{1}{2} \int \left\{ g(h-d)^2 \,+\, h|\boldsymbol{\nabla}\bar{\phi}|^2 \,-\, \frac{h\,[\,\partial_t d \,+\, \boldsymbol{\nabla}\bar{\phi}\boldsymbol{\cdot}\boldsymbol{\nabla} d\,]^2}{1 \,+\, |\boldsymbol{\nabla} d|^2} \right\} \mathrm{d}^2\boldsymbol{x}. \tag{2.18}$$

One can easily check, after computing the variations, that the Hamiltonian (2.18) yields

$$\partial_t\, h \;=\; -\,\boldsymbol{\nabla}\boldsymbol{\cdot} \left[h\boldsymbol{\nabla}\bar{\phi} \;-\; \frac{\partial_t d \,+\, \boldsymbol{\nabla}\bar{\phi}\boldsymbol{\cdot}\boldsymbol{\nabla} d}{1 + |\boldsymbol{\nabla} d|^2}\, h\, \boldsymbol{\nabla} d \right],$$

$$\partial_t\, \bar{\phi} \;=\; -\, g(h-d) \;-\; \tfrac{1}{2}|\boldsymbol{\nabla}\bar{\phi}|^2 \;+\; \frac{[\,\partial_t d \,+\, \boldsymbol{\nabla}\bar{\phi}\boldsymbol{\cdot}\boldsymbol{\nabla} d\,]^2}{1 + |\boldsymbol{\nabla} d|^2},$$

which are equivalent to the system (2.9) – (2.11).

Remark 4. *If we rewrite Hamiltonian (2.18) in the following equivalent form:*

$$\mathcal{H} \;=\; \tfrac{1}{2} \int \left\{\, g\,\eta^2 \;+\; h\,\bar{\boldsymbol{u}}^2 \;+\; h\,(\check{v} + \partial_t d)^2 \;-\; h\,(\partial_t d)^2 \,\right\} \mathrm{d}^2\boldsymbol{x}, \tag{2.19}$$

one can see that Hamiltonian (2.18) is actually positive definite if the bottom is static, i.e., $d = d(x)$ or $\partial_t d = 0$. In other words if there is no external input of energy into the system.

Moreover, the Hamiltonian structure of the classical Saint-Venant equations can be recovered substituting $\check{v} = 0$ into the last Hamiltonian (2.19):

$$\mathcal{H}_0 \;=\; \tfrac{1}{2} \int \left\{\, g\,\eta^2 \;+\; h\,\bar{\boldsymbol{u}}^2 \,\right\} \mathrm{d}^2\boldsymbol{x}.$$

2.3. **Steady solutions.** We consider here the two-dimensional case in the perspective to derive a closed form solution for a steady state flow over a general bathymetry. We assume the following upstream conditions at $x \to -\infty$:

$$\eta \;\to\; 0, \qquad d \;\to\; d_0, \qquad \bar{u} \;\to\; u_0 \;\geqslant\; 0.$$

Physically, these conditions mean that far upstream we consider a uniform current over a horizontal bottom. The mass conservation in steady condition yields

$$h\,\bar{u} \;=\; d_0\, u_0,$$

while the momentum conservation equation becomes

$$g\,h \;+\; \tfrac{1}{2}\,\bar{u}^2 \left[\,1 + (\partial_x d)^2\,\right] \;=\; g\,d_0 \;+\; \tfrac{1}{2}\,u_0^2.$$

Combining the last two relations yields the following cubic equations for the total water depth

$$g\,h^3 \;-\; (\,g\,d_0 \,+\, \tfrac{1}{2}\,u_0^2\,)\,h^2 \;+\; \tfrac{1}{2}\,(\,d_0\,u_0\,)^2\,[\,(1 \,+\, (\partial_x d)^2\,] \;=\; 0. \tag{2.20}$$

As it is well known, a cubic equation has three (in general complex) roots. From physical interpretation of h, we are only interested in real positive roots.

Remark 5. *It is straightforward to derive a similar equation for steady solutions to the classical Saint-Venant equations*

$$g\,h^3 \;-\; (\,g\,d_0 \;+\; \tfrac{1}{2}\,u_0^2\,)\,h^2 \;+\; \tfrac{1}{2}\,(\,d_0\,u_0\,)^2 \;=\; 0.$$

The last relation can be also obtained from equation (2.20) by taking $\partial_x d = 0$. Consequently, we can say that steady solutions to classical Saint-Venant equations do not take into account the bottom slope local variations.

One solution of (2.20) is

$$h \;=\; d_0 \big/ \big[\,A\,C^{-1/3} \;+\; \tfrac{1}{3}\,C^{1/3}\,\big]\,, \qquad C \;\equiv\; 3\sqrt{B^2 \;-\; 3\,A^3} \;-\; 3\,B, \tag{2.21}$$

with

$$A(x) \;\equiv\; \frac{1 \;+\; 2\,g\,d_0\,u_0^{-2}}{1 \;+\; (\partial_x d)^2} \;\geqslant\; 0, \qquad B(x) \;\equiv\; \frac{9\,g\,d_0\,u_0^{-2}}{1 \;+\; (\partial_x d)^2} \;\geqslant\; 0.$$

This solution is real only if $B^2 \geqslant 3A^3$ (in that case equation (2.20) has only one real root) or equivalently if

$$27\,F^{\,2}\,(\partial_x d)^2 \;-\; (F^{\,2} - 1)^2\,(F^{\,2} + 8) \;\geqslant\; 0, \qquad F \;\equiv\; u_0 \,/\, \sqrt{g\,d_0}\,,$$

where F is a Froude number. In the case of the classical Saint-Venant equations (i.e., taking $\partial_x d = 0$), the last condition is satisfied only for the critical regime $F = 1$. In the modified model solution, (2.21) is real in a vicinity of $F = 1$, which depends on the magnitude of the bottom local slope $\partial_x d$. However, if this solution is real, it is necessary negative — see the definition of C in (2.21). Hence, it is unphysical and must be rejected. In other words it means that under condition $B^2 > 3A^3$, the flow cannot be steady. Physically, a singularity such as wave breaking does not allow the flow to reach the steady state.

If $B^2 < 3A^3$, the equation (2.20) has three real roots, two of them being positive. The first root $h = h^+$ corresponds to the subcritical regime:

$$h^+ \;=\; d_0 \Big/ \Big[\,2\,\sqrt{A/3}\,\cos\!\big(\tfrac{1}{3}\arccos\big(-3^{-1/2}BA^{-3/2}\big) \;-\; \tfrac{2}{3}\pi\big)\Big]\,,$$

and one supercritical root $h = h^-$:

$$h^- \;=\; d_0 \Big/ \Big[\,2\,\sqrt{A/3}\,\cos\!\big(\tfrac{1}{3}\arccos\big(-3^{-1/2}BA^{-3/2}\big)\big)\Big]\,.$$

We note that $h^- < h^+$.

Finally, in the limiting case $B^2 = 3A^3$, for a given Froude number F, there is only one absolute value of the slope for which this identity is satisfied, that is

$$(\partial_x d)^2 \;=\; (F^{\,2} - 1)^2\,(F^{\,2} + 8)\,/\,(26F^{\,2}). \tag{2.22}$$

For instance, if $\partial_x d = 0$ then $B^2 = 3A^3$ if and only if $F = 1$.

Gravity acceleration g:	$1\,\mathrm{m\,s^{-2}}$
Undisturbed water depth d_0:	$1\,\mathrm{m}$
Deformation amplitude a:	$0.5\,\mathrm{m}$
Half-length of the uplift area b:	$2.5\,\mathrm{m}$
Upstream flow speed, u_0	$2.0\,\mathrm{m\,s^{-1}}$

TABLE 1. Values of various parameters used for the steady state computation.

Consider now the opposite case when the slope is given $d_x \neq 0$. In this case condition (2.22) is satisfied for two values of the Froude number $F = F^{\pm}$:

$$(F^-)^2 = 6\sqrt{1+(\partial_x d)^2}\cos\bigl(\tfrac{1}{3}\arccos\bigl(-[1+(\partial_x d)^2]^{-1/2}\bigr) - \tfrac{2}{3}\pi\bigr) - 2 \leqslant 1,$$
$$(F^+)^2 = 6\sqrt{1+(\partial_x d)^2}\cos\bigl(\tfrac{1}{3}\arccos\bigl(-[1+(\partial_x d)^2]^{-1/2}\bigr)\bigr) - 2 \geqslant 1.$$

If $F^- < F < F^+$, we have $B^2 > 3A^3$ and there are no steady states. Therefore, we must have $F \leqslant F^-$ or $F \geqslant F^+$.

In order to illustrate the developments made above, we compute a steady flow over a bump. The bottom takes the form

$$d(x) = d_0 - a\,b^{-4}\left(x^2 - b^2\right)^2 \mathrm{H}(b^2 - x^2),$$

where $\mathrm{H}(x)$ is the Heaviside step function [1], a and b being the bump amplitude and its half-length, respectively. The values of various parameters are given in Table 1. We consider here for illustrative purposes the supercritical case for the classical and new models. The result are shown on Figure 2 where some small differences can be noted with respect to the classical Saint-Venant equations.

3. Numerical methods

In this Section we discuss some properties of the system (2.12), (2.13) and then, we propose a space discretization procedure based on the finite volume method along with a high-order adaptive time stepping.

3.1. Hyperbolic structure.

From now on, we consider equations (2.12), (2.13) posed in one horizontal space dimension for simplicity:

$$\partial_t h + \partial_x [h\,\bar{u}] = 0, \tag{3.1}$$
$$\partial_t [\bar{u} - \check{v}\,\partial_x d] + \partial_x \left[g\,\eta + \tfrac{1}{2}\bar{u}^2 + \tfrac{1}{2}\check{v}^2 + \check{v}\,\partial_t d\right] = 0. \tag{3.2}$$

In order to make appear conservative variables we will introduce the potential velocity variable $U = \partial_x\bar{\phi}$. From equation (2.10) it is straightforward to see that U satisfies the relation

$$U = \bar{u} - \check{v}\,\partial_x d,$$

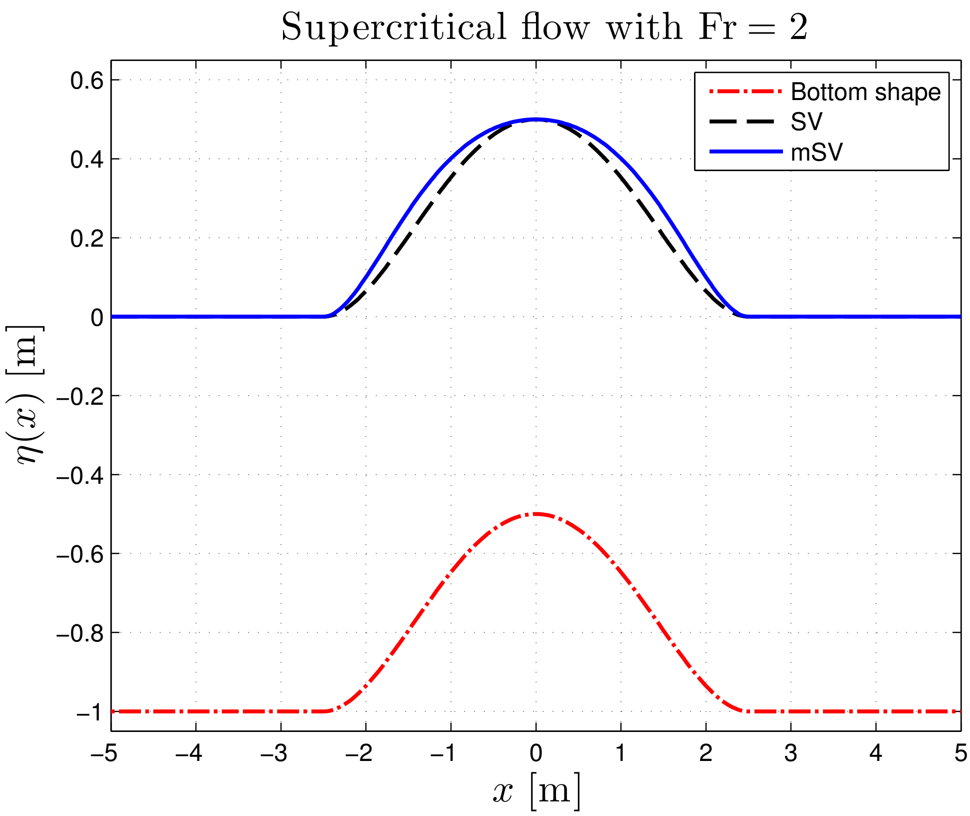

FIGURE 2. Supercritical steady state solutions over a bump for the Froude number $F = 2$. Comparison between the classical and modified Saint-Venant equations.

Depth averaged and vertical bottom velocities can be also easily expressed in terms of the potential velocity U

$$\bar{u} \;=\; \frac{U \,-\, (\partial_t d)\,(\partial_x d)}{1 \,+\, (\partial_x d)^2}, \qquad \check{v} \;=\; -\frac{\partial_t d \,+\, U\,\partial_x d}{1 \,+\, (\partial_x d)^2}.$$

Consequently, using this new variable equations (3.1), (3.2) can be rewritten as a system of conservation laws

$$\partial_t\, h \;+\; \partial_x \left[h\, \frac{U \,-\, (\partial_t d)\,(\partial_x d)}{1 \,+\, (\partial_x d)^2} \right] \;=\; 0,$$

$$\partial_t\, U \;+\; \partial_x \left[g\,(h - d) \,+\, \frac{1}{2}\frac{U^2 \,-\, 2\,U\,(\partial_t d)\,(\partial_x d) - (\partial_t d)^2}{1 \,+\, (\partial_x d)^2} \right] \;=\; 0.$$

For the sake of simplicity, we rewrite the above system in the following quasilinear vectorial form:

$$\partial_t\, w \;+\; \partial_x\, f(w) \;=\; 0, \tag{3.3}$$

where we introduced the vector of conservative variables w and the advective flux $f(w)$:

$$w = \begin{pmatrix} h \\ U \end{pmatrix}, \qquad f(w) = \begin{pmatrix} h\dfrac{U - (\partial_t d)(\partial_x d)}{1 + (\partial_x d)^2} \\ g(h-d) + \dfrac{U^2 - 2U(\partial_x d)(\partial_t d) - (\partial_t d)^2}{2\,[1 + (\partial_x d)^2]} \end{pmatrix}.$$

The Jacobian matrix of the advective flux $f(w)$ can be easily computed:

$$\mathbb{A}(w) = \frac{\partial\, f(w)}{\partial w} = \frac{1}{1 + (\partial_x d)^2} \begin{bmatrix} U - (\partial_t d)(\partial_x d) & h \\ g\,(1 + (\partial_x d)^2) & U - (\partial_t d)(\partial_x d) \end{bmatrix} = \begin{bmatrix} \bar{u} & \dfrac{h}{1 + (\partial_x d)^2} \\ g & \bar{u} \end{bmatrix}.$$

The matrix $\mathbb{A}(w)$ has two distinct eigenvalues:

$$\lambda^{\pm} = \frac{U - (\partial_t d)\,(\partial_x d)}{1 + (\partial_x d)^2} \pm c = \bar{u} \pm c, \qquad c^2 \equiv \frac{g\,h}{1 + (\partial_x d)^2}.$$

Remark 6. *Physically, the quantity c represents the phase celerity of long gravity waves. In the framework of the Saint-Venant equations, it is well known that $c = \sqrt{gh}$. Both expressions differ by the factor $\sqrt{1 + (\partial_x d)^2}$. In our model, the long waves are slowed down by strong bathymetric variations since fluid particles are constrained to follow the seabed.*

Right and left eigenvectors coincide with those of the Saint-Venant equations and they are given by the following matrices

$$R = \begin{bmatrix} -h & h \\ \sqrt{gh} & \sqrt{gh} \end{bmatrix}, \qquad L = \frac{1}{2} \begin{bmatrix} -h^{-1} & (gh)^{-1/2} \\ h^{-1} & (gh)^{-1/2} \end{bmatrix}.$$

Columns of the matrix R constitute eigenvectors corresponding to eigenvalues λ^- and λ^+ respectively. Corresponding left eigenvectors are conventionally written in lines of the matrix L.

3.2. **Group velocity.** We would like to compute also the group velocity in the framework of the modified Saint-Venant equations. This quantity is traditionally associated to the wave energy propagation speed [73, 28]. Recall, that in the classical linearized shallow water theory, the phase c and group c_g velocities are equal [73]:

$$c = \frac{\omega}{k} = \sqrt{gh}, \qquad c_g = \frac{\mathrm{d}\,\omega}{\mathrm{d}k} = \sqrt{gh},$$

where $\omega = k\sqrt{gh}$ is the dispersion relation for linear long waves, k being the wavenumber and ω being the angular frequency.

In order to assess the wave energy propagation speed we will consider a quasilinear system of equations composed of mass and energy conservation laws:

$$\partial_t h + \partial_x \left[h\,\frac{U - (\partial_x d)(\partial_t d)}{1 + (\partial_x d)^2} \right] = 0,$$

$$\partial_t E + \partial_x \left[(E + \tfrac{1}{2} g h^2) \frac{U - (\partial_x d)(\partial_t d)}{1 + (\partial_x d)^2} \right] = -(g + \gamma)\,h\,\partial_t d,$$

where γ is defined in (2.16) and E is the total energy considered already above (2.17):

$$E \;=\; h\,\frac{\bar{u}^2 + \check{v}^2}{2} \;+\; \frac{g\,(\eta^2 - d^2)}{2} \;=\; \frac{h}{2}\,\frac{U^2 + (\partial_t d)^2}{1 \,+\, (\partial_x d)^2} \;+\; \frac{g\,(h^2 - 2hd)}{2}.$$

The last formula can be inverted to express the potential velocity in terms of the wave energy:

$$U^2 \;=\; [\,1 \,+\, (\partial_x d)^2\,]\left(\frac{2E}{h} \,-\, gh \,+\, 2gd\right) \,-\, (\partial_t d)^2.$$

In the spirit of computations performed in the previous section, we compute the Jacobian matrix $\mathbb{J}$ of the mass-energy advection operator:

$$\mathbb{J} \;=\; \frac{1}{1 \,+\, (\partial_x d)^2}\begin{bmatrix} U \,-\, (\partial_x d)(\partial_t d) \,+\, h\dfrac{\partial U}{\partial h} & h\dfrac{\partial U}{\partial E} \\ gh[U - (\partial_x d)(\partial_t d)] \,+\, (E + \frac{1}{2}gh^2)\dfrac{\partial U}{\partial h} & U \,-\, (\partial_x d)(\partial_t d) \,+\, (E + \frac{1}{2}gh^2)\dfrac{\partial U}{\partial E} \end{bmatrix},$$

where partial derivatives are given here:

$$\frac{\partial U}{\partial h} \;=\; -[\,1 \,+\, (\partial_x d)^2\,]\,\frac{gh^2 \,+\, 2E}{2\,h^2\,U}, \qquad \frac{\partial U}{\partial E} \;=\; \frac{1 \,+\, (\partial_x d)^2}{h\,U}.$$

Computation of the Jacobian $\mathbb{J}$ eigenvalues leads the following expression for the group velocity of the modified Saint-Venant equations:

$$c_g^2 \;=\; \frac{g\,h}{1 \,+\, (\partial_x d)^2}\,\frac{U \,-\, (\partial_x d)(\partial_t d)}{U}.$$

The last formula is very interesting. It means that in the moving bottom case, the group velocity c_g is modified and does not coincide anymore with the phase velocity $c^2 = gh[1 + (\partial_x d)^2]^{-1}$. This fact represents another new and non-classical feature of the modified Saint-Venant equations. The relative difference between phase and group velocities squared is

$$\frac{c^2 \,-\, c_g^2}{c^2} \;=\; \frac{(\partial_x d)\,(\partial_t d)}{U}, \tag{3.4}$$

which is not necessarily always positive. When it is negative, the energy is injected into the system at a higher rate than can be spreaded, thus leading to enenergy accumulation and possibly favouring the breaking events.

3.3. **Finite volume scheme.** Let us fix a partition of $\mathbb{R}$ into cells (or finite volumes) $\mathcal{C}_i = [x_{i-\frac{1}{2}}, x_{i+\frac{1}{2}}]$ with cell center $x_i = \frac{1}{2}(x_{i-\frac{1}{2}} + x_{i+\frac{1}{2}})$, $i \in \mathbb{Z}$. Let Δx_i denotes the length of the cell $\mathcal{C}_i$. Without any loss of generality we assume the partition to be uniform, i.e., $\Delta x_i = \Delta x$, $\forall i \in \mathbb{Z}$. The solution $w(x,t)$ is approximated by discrete values and, in order to do so, we introduce the cell average of w over the cell $\mathcal{C}_i$, i.e.,

$$\bar{w}_i(t) \;\equiv\; \frac{1}{\Delta h}\int_{\mathcal{C}_i} w(x,t)\,\mathrm{d}x.$$

A simple integration of (3.3) over the cell $\mathcal{C}_i$ leads the following exact relation

$$\frac{\mathrm{d}\,\bar{w}_i}{\mathrm{d}t} \;+\; \frac{f\Big(w(x_{i+\frac{1}{2}}, t)\Big) \,-\, f\Big(w(x_{i-\frac{1}{2}}, t)\Big)}{\Delta x} \;=\; 0.$$

Since the discrete solution is discontinuous at cell the interfaces $x_{i+\frac{1}{2}}$, $i \in \mathbb{Z}$, the heart of the matter in the finite volume method is to replace the flux through cell faces by the so-called numerical flux function

$$f\left(w(x_{i\pm\frac{1}{2}}, t)\right) \;\approx\; \mathcal{F}_{i\pm\frac{1}{2}}\left(\bar{w}^L_{i\pm\frac{1}{2}}, \bar{w}^R_{i\pm\frac{1}{2}}\right),$$

where $\bar{w}^{L,R}_{i\pm\frac{1}{2}}$ are reconstructions of conservative variables $\bar{w}$ from left and right sides of each cell interface [8, 80]. The reconstruction procedure employed in the present study is described below.

In order to discretise the advective flux $f(w)$, we use the so-called FVCF scheme [39, 40]

$$\mathcal{F}(v, w) \;=\; \frac{f(v) \,+\, f(w)}{2} \;-\; \mathcal{S}(v, w)\, \frac{f(w) \,-\, f(v)}{2}.$$

The first part of the numerical flux $\mathcal{F}(v, w)$ is centred, while the second part is the upwinding introduced according to local waves propagation directions

$$\mathcal{S}(v, w) \;=\; \mathrm{sign}\left(\mathbb{A}\left(\frac{v + w}{2}\right)\right), \quad \mathrm{sign}(\mathbb{A}) \;=\; R \cdot \mathrm{diag}(s^-, s^+) \cdot L, \quad s^\pm \;\equiv\; \mathrm{sign}(\lambda^\pm).$$

After some simple algebraic computations one can find expressions for sign matrix $\mathcal{S}$ coefficients

$$\mathcal{S} \;=\; \frac{1}{2}\begin{bmatrix} (s^+ + s^-) & (s^+ - s^-)\sqrt{h/g} \\ (s^+ - s^-)\sqrt{g/h} & (s^+ + s^-) \end{bmatrix},$$

all coefficients being evaluated at the average state of left and right face values.

Taking into account the developments presented above, the semi-discrete scheme takes the form

$$\frac{\mathrm{d}\,\bar{w}_i}{\mathrm{d}t} \;+\; \frac{\mathcal{F}_{i+\frac{1}{2}}\left(\bar{w}^L_{i+\frac{1}{2}}, \bar{w}^R_{i+\frac{1}{2}}\right) - \mathcal{F}_{i-\frac{1}{2}}\left(\bar{w}^L_{i-\frac{1}{2}}, \bar{w}^R_{i-\frac{1}{2}}\right)}{\Delta x} \;=\; 0. \tag{3.5}$$

The discretisation in time of the last system of ODEs is discussed in Section 3.5. Meanwhile, we present the employed reconstruction procedure.

3.4. **High-order reconstruction.** In order to obtain a higher-order scheme in space, we need to replace the piecewise constant data by a piecewise polynomial representation. This goal is achieved by various so-called reconstruction procedures, such as MUSCL TVD [51, 79, 80], UNO [46], ENO [45], WENO [85] and many others. In our previous study on Boussinesq-type equations [32], the UNO2 scheme showed a good performance with low dissipation in realistic propagation and runup simulations. Consequently, we retain this scheme for the discretisation of the modified Saint-Venant equations.

Remark 7. *In TVD schemes, the numerical operator is required (by definition) not to increase the total variation of the numerical solution at each time step. It follows that the value of an isolated maximum may only decrease in time which is not a good property for the simulation of coherent structures such as solitary waves. The non-oscillatory UNO2 scheme, employed in our study, is only required to diminish the* number *of local extrema in the numerical solution. Unlike TVD schemes, UNO schemes are not constrained to damp the values of each local extremum at every time step.*

The main idea of the UNO2 scheme is to construct a non-oscillatory piecewise-parabolic interpolant $Q(x)$ to a piecewise smooth function $w(x)$ (see [46] for more details). On each segment containing the face $x_{i+\frac{1}{2}} \in [x_i, x_{i+1}]$, the function $Q(x) = q_{i+\frac{1}{2}}(x)$ is locally a quadratic polynomial $q_{i+\frac{1}{2}}(x)$ and wherever $w(x)$ is smooth we have

$$Q(x) \;-\; w(x) \;=\; \mathcal{O}(\Delta x^3), \qquad \frac{\mathrm{d}\,Q}{\mathrm{d}x}(x \pm 0) \;-\; \frac{\mathrm{d}\,w}{\mathrm{d}x} \;=\; \mathcal{O}(\Delta x^2).$$

Also $Q(x)$ should be non-oscillatory in the sense that the number of its local extrema does not exceed that of $w(x)$. Since $q_{i+\frac{1}{2}}(x_i) = \bar{w}_i$ and $q_{i+\frac{1}{2}}(x_{i+1}) = \bar{w}_{i+1}$, it can be written in the form

$$q_{i+\frac{1}{2}}(x) \;=\; \bar{w}_i \;+\; d_{i+\frac{1}{2}}(w)\,\frac{x - x_i}{\Delta x} \;+\; \tfrac{1}{2} D_{i+\frac{1}{2}} w \cdot \frac{(x - x_i)(x - x_{i+1})}{\Delta x^2},$$

where $d_{i+\frac{1}{2}}(w) \equiv \bar{w}_{i+1} - \bar{w}_i$ and $D_{i+\frac{1}{2}} v$ is closely related to the second derivative of the interpolant since $D_{i+\frac{1}{2}} v = \Delta x^2 q''_{i+\frac{1}{2}}(x)$. The polynomial $q_{i+\frac{1}{2}}(x)$ is chosen to be one the least oscillatory between two candidates interpolating $w(x)$ at (x_{i-1}, x_i, x_{i+1}) and (x_i, x_{i+1}, x_{i+2}). This requirement leads to the following choice of $D_{i+\frac{1}{2}} v$

$$D_{i+\frac{1}{2}} w := \mathrm{minmod}\bigl(D_i w, D_{i+1} w\bigr), \quad D_i w = \bar{w}_{i+1} - 2\bar{w}_i + \bar{w}_{i-1}, \quad D_{i+1} w = \bar{w}_{i+2} - 2\bar{w}_{i+1} + \bar{w}_i,$$

and $\mathrm{minmod}(x, y)$ is the usual min mod function defined as:

$$\mathrm{minmod}(x, y) \;=\; \tfrac{1}{2}\,[\,\mathrm{sign}(x) \;+\; \mathrm{sign}(y)\,] \times \min(|x|, |y|).$$

To achieve the second order $\mathcal{O}(\Delta x^2)$ accuracy, it is sufficient to consider piecewise linear reconstructions in each cell. Let $L(x)$ denote this approximately reconstructed function which can be written in the form

$$L(x) \;=\; \bar{w}_i \;+\; s_i\,(x - x_i)\,/\,\Delta x, \qquad x_{i-\frac{1}{2}} \leqslant x \leqslant x_{i+\frac{1}{2}}.$$

To make $L(x)$ a non-oscillatory approximation, we use the parabolic interpolation $Q(x)$ constructed below to estimate the slopes s_i within each cell

$$s_i \;=\; \Delta x \times \mathrm{minmod}\left(\left.\frac{\mathrm{d}\,Q}{\mathrm{d}x}\right|_{x = x_i^-}, \left.\frac{\mathrm{d}\,Q}{\mathrm{d}x}\right|_{x = x_i^+}\right).$$

In other words, the solution is reconstructed on the cells while the solution gradient is estimated on the dual mesh as it is often performed in more modern schemes [7, 8]. A brief summary of the UNO2 reconstruction can be also found in [32].

3.5. **Time stepping.** We rewrite the semi-discrete scheme (3.5) as a system of ODEs:

$$\partial_t\,\bar{w} \;=\; \mathcal{L}(\bar{w}, t), \qquad \bar{w}(0) \;=\; \bar{w}_0.$$

In order to solve numerically the last system of equations, we apply the Bogacki–Shampine method [10]. It is a third-order Runge–Kutta scheme with four stages. It has an embedded second order method which is used to estimate the local error and, thus, to adapt the time step size. Moreover, the Bogacki–Shampine method enjoys the First Same As Last (FSAL) property so that it needs three function evaluations per step. This method is also

implemented in the `ode23` function in MATLAB [68]. A step of the Bogacki–Shampine method is given by

$$\begin{aligned}
k_1 &= \mathcal{L}(\bar{w}^{(n)}, t_n), \\
k_2 &= \mathcal{L}(\bar{w}^{(n)} + \tfrac{1}{2}\Delta t_n k_1, t_n + \tfrac{1}{2}\Delta t), \\
k_3 &= \mathcal{L}(\bar{w}^{(n)}) + \tfrac{3}{4}\Delta t_n k_2, t_n + \tfrac{3}{4}\Delta t), \\
\bar{w}^{(n+1)} &= \bar{w}^{(n)} \;+\; \Delta t_n \left(\tfrac{2}{9}k_1 + \tfrac{1}{3}k_2 + \tfrac{4}{9}k_3\right), \\
k_4 &= \mathcal{L}(\bar{w}^{(n+1)}, t_n + \Delta t_n), \\
\bar{w}_2^{(n+1)} &= \bar{w}^{(n)} \;+\; \Delta t_n \left(\tfrac{4}{24}k_1 + \tfrac{1}{4}k_2 + \tfrac{1}{3}k_3 + \tfrac{1}{8}k_4\right).
\end{aligned}$$

Here $\bar{w}^{(n)} \approx \bar{w}(t_n)$, Δt is the time step and $\bar{w}_2^{(n+1)}$ is a second order approximation to the solution $\bar{w}(t_{n+1})$, so the difference between $\bar{w}^{(n+1)}$ and $\bar{w}_2^{(n+1)}$ gives an estimation of the local error. The FSAL property consists in the fact that k_4 is equal to k_1 in the next time step, thus saving one function evaluation.

If the new time step Δt_{n+1} is given by $\Delta t_{n+1} = \rho_n \Delta t_n$, then according to H211b digital filter approach [69, 70], the proportionality factor ρ_n is given by:

$$\rho_n \;=\; \left(\frac{\delta}{\varepsilon_n}\right)^{\beta_1} \left(\frac{\delta}{\varepsilon_{n-1}}\right)^{\beta_2} \rho_{n-1}^{-\alpha}, \tag{3.6}$$

where ε_n is a local error estimation at time step t_n and constants β_1, β_2 and α are defined as

$$\alpha \;=\; 1\,/\,4, \qquad \beta_1 \;=\; \beta_2 \;=\; 1\,/\,4\,p.$$

The parameter p is the order of the scheme ($p = 3$ in our case).

Remark 8. *The adaptive strategy (3.6) can be further improved if we smooth the factor ρ_n before computing the next time step Δt_{n+1}*

$$\Delta t_{n+1} \;=\; \hat{\rho}_n \, \Delta t_n, \qquad \hat{\rho}_n \;=\; \omega(\rho_n).$$

The function $\omega(\rho)$ is called the time step limiter *and should be smooth, monotonically increasing and should satisfy the following conditions*

$$\omega(0) \;<\; 1, \qquad \omega(+\infty) \;>\; 1, \qquad \omega(1) \;=\; 1, \omega'(1) \;=\; 1.$$

One possible choice is suggested in [70]:

$$\omega(\rho) \;=\; 1 \;+\; \kappa \arctan\!\left(\frac{\rho - 1}{\kappa}\right).$$

In our computations the parameter κ is set to 1.

Initial wavenumber κ:	$1\,\mathsf{m}^{-1}$
Gravity acceleration g:	$1\,\mathsf{m\,s}^{-2}$
Final simulation time T:	$24\,\mathsf{s}$
Initial wave amplitude b:	$0.2\,\mathsf{m}$
Undisturbed water depth d_0:	$1\,\mathsf{m}$
Bathymetry oscillation amplitude a:	$0.1\,\mathsf{m}$
Low bathymetry oscillation wavelength k_1:	$2\,\mathsf{m}^{-1}$
High bathymetry oscillation wavelength k_2:	$6\,\mathsf{m}^{-1}$

Table 2. Values of various parameters used for the wave propagation over an oscillatory bottom test-case.

4. Numerical results

The numerical scheme presented above has already been validated in several studies even in the case of dispersive waves [32, 31]. Consequently, we do not present here the standard convergence tests which can be found in references cited above. In the present Section we show numerical results which illustrate some properties of modified Saint-Venant equations with respect to their classical counterpart.

In the sequel we consider only one-dimensional case for simplicity. The physical domain will be also limited by wall-boundary conditions. Other types of boundary conditions obviously could also be considered.

4.1. Wave propagation over oscillatory bottom.

We begin the exposition of numerical results by presenting a simple test-case of a wave propagation over a static but highly oscillatory bottom. Let us consider a one-dimensional physical domain $[-10, 10]$ which is discretized into $N = 350$ equal control volumes. The tolerance parameter δ in the time stepping algorithm is chosen to be 10^{-4}. The initial condition will be simply a bump localised near the center $x = 0$ and posed on the free surface with initial zero velocity field

$$\eta_0(x) \;=\; b\,\mathrm{sech}^2(\kappa x), \qquad u_0(x) \;=\; 0.$$

The bottom is given analytically by the function

$$d(x) \;=\; d_0 \;+\; a\sin(kx).$$

In other words, the bathymetry function $d(x)$ consists of uniform level d_0 which is perturbed by uniform oscillations of amplitude a. Since the bathymetry is static, the governing equations (3.1) and (3.2) are simplified at some point.

Hereafter, we fix two wavenumbers k_1 and k_2 ($k_1 < k_2$) and perform a comparison between numerical solutions to the classical and modified Saint-Venant equations. The main idea behind this comparison is to show the similarity between two solutions for mild bottoms and, correspondingly, to highlight the differences for stronger gradients. The values of various physical parameters used in numerical simulations are given in Table 2.

Several snapshots of the free surface elevation during the wave propagation test-case are presented on Figures 3 – 9. The left image refers to the mild bottom gradient case ($k_1 = 2$)

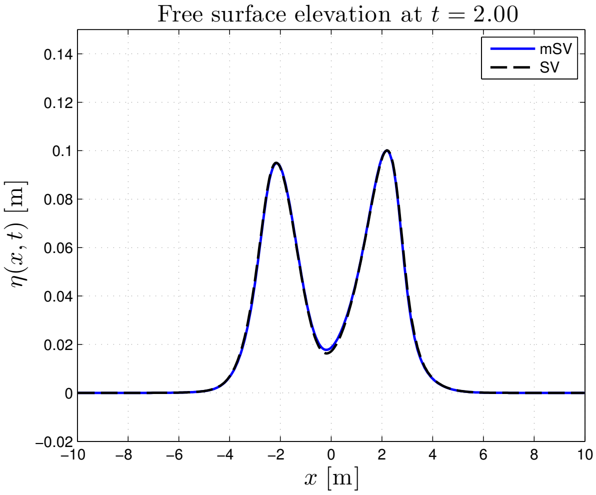

(a) Low oscillations, k_1

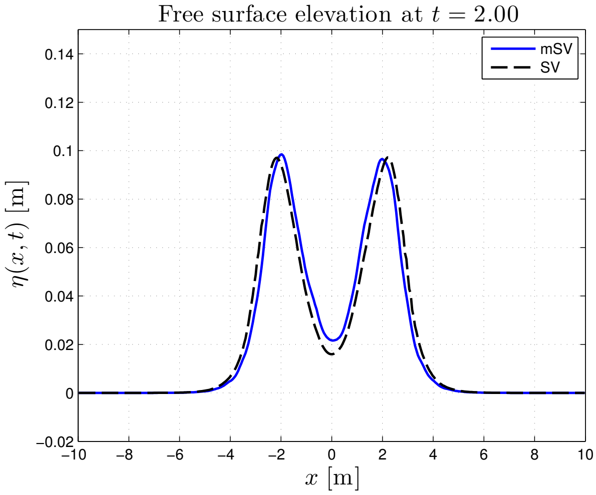

(b) High oscillations, k_2

FIGURE 3. Wave propagation over an oscillatory bottom, $t = 2\,\mathsf{s}$.

while the right image corresponds to the oscillating bottom ($k_2 = 6$). Everywhere, the solid blue line represents a solution to the modified Saint-Venant equations, while the dotted black line refers to the classical solution.

Numerical results on left images indicate that both models give very similar results when bathymetry gradients are gentle. Two solutions are almost indistinguishable to grahic resolutions, especially at the beginning. However, some divergences are accumulated with time. At the end of the simulation some differences become to be visible to the graphic resolution. On the other hand, numerical solutions on right images are substantially different from first instants of the wave propagation. In accordance with theoretical predictions (see Remark 6), the wave in modified Saint-Venant equations propagates with speed effectively reduced by bottom oscillations. This fact explains a certain lag between two numerical solutions in the highly oscillating case. We note that the wave shape is also different in classical and improved equations.

Finally, on Figure 10 we show the evolution of the local time step during the simulation. It can be easily seen that the time adaptation algorithm very quickly finds the optimal value of the time step which is then maintained during the whole simulation. This observation is even more flagrant on the right image corresponding to the highly oscillating case.

4.2. **Wave generation by sudden bottom uplift.** We continue to investigate various properties of the modified Saint-Venant equations. In this section, we present a simple test-case which involves the bottom motion. More precisely, we will investigate two cases of slow and fast uplifts of a portion of bottom. This simple situation has some important implications to tsunami genesis problems [43, 78, 29, 27, 50, 23, 57, 24].

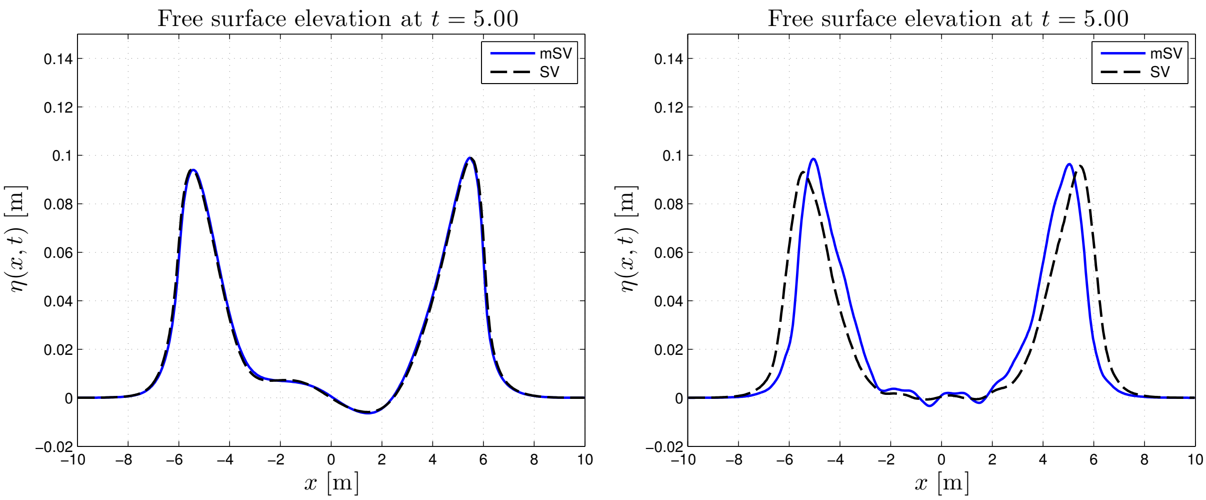

(a) Low oscillations, k_1 (b) High oscillations, k_2

FIGURE 4. Wave propagation over an oscillatory bottom, $t = 5\,\mathsf{s}$.

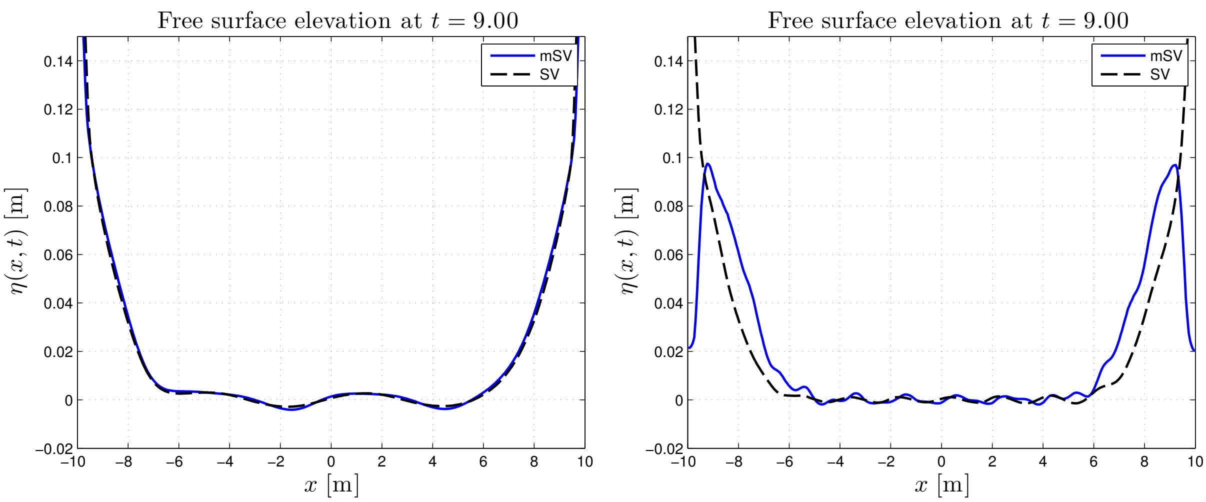

(a) Low oscillations, k_1 (b) High oscillations, k_2

FIGURE 5. Wave propagation over an oscillatory bottom, $t = 9\,\mathsf{s}$.

The physical domain and discretisation parameters are inherited from the last section. The bottom is given by the following function:

$$d(x,t) \;=\; d_0 \;-\; a\,T(t)\,\mathrm{H}(b^2 - x^2)\left[\left(\frac{x}{b}\right)^2 - 1\right]^2, \qquad T(t) \;=\; 1 \;-\; \mathrm{e}^{-\alpha t},$$

where $\mathrm{H}(x)$ is the Heaviside step function [1], a is the deformation amplitude and b is the half-length of the uplifting sea floor area. The function $T(t)$ provides us a complete information on the dynamics of the bottom motion. In tsunami wave literature, it is called

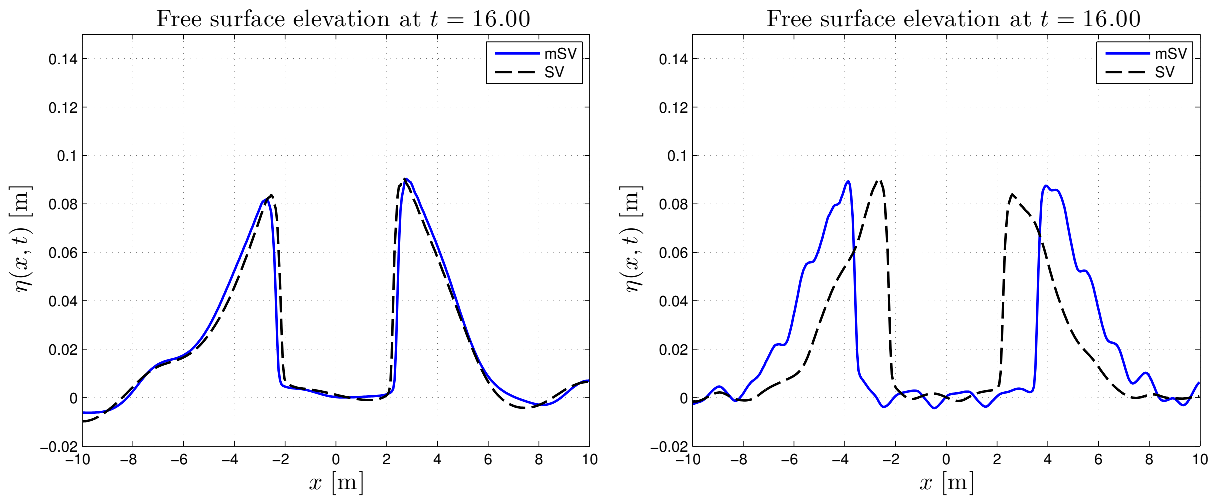

(a) Low oscillations, k_1 (b) High oscillations, k_2

FIGURE 6. Wave propagation over an oscillatory bottom, $t = 16\,\mathsf{s}$.

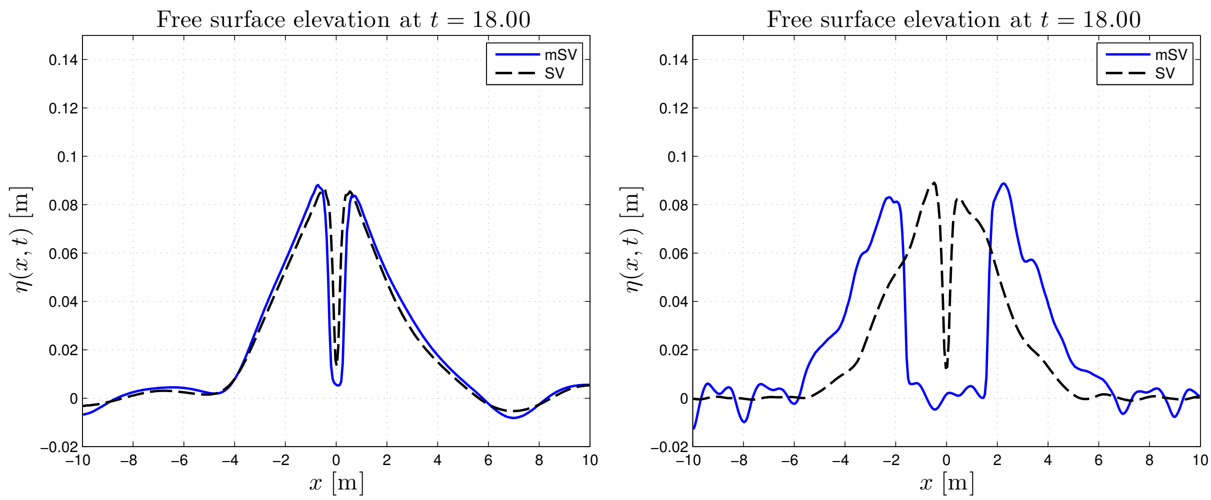

(a) Low oscillations, k_1 (b) High oscillations, k_2

FIGURE 7. Wave propagation over an oscillatory bottom, $t = 18\,\mathsf{s}$.

a *dynamic scenario* [44, 43, 27, 50, 23]. Obviously, other choices of the time dependence are possible. Initially the free surface is undisturbed and the velocity field is taken to be identically zero. The values of various parameter are given in Table 3.

Numerical results of the moving bottom test-case are shown on Figures 11–16. On all these images the blue solid line corresponds to the modified Saint-Venant equations, while the black dashed line refers to its classical counterpart. The dash-dotted line shows the bottom profile which evolves in time as well.

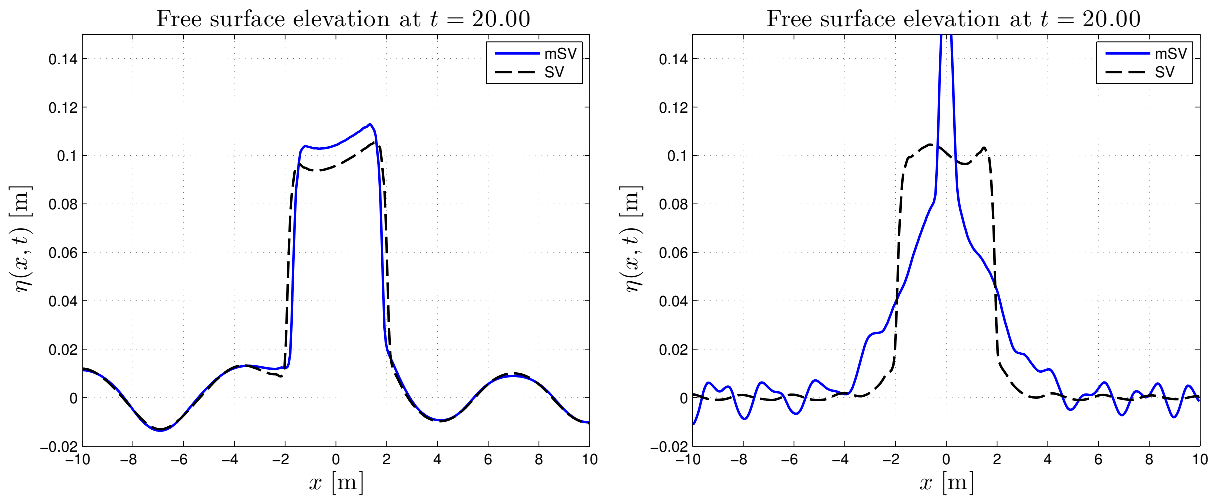

(a) Low oscillations, k_1 (b) High oscillations, k_2

FIGURE 8. Wave propagation over an oscillatory bottom, $t = 20\,\mathsf{s}$.

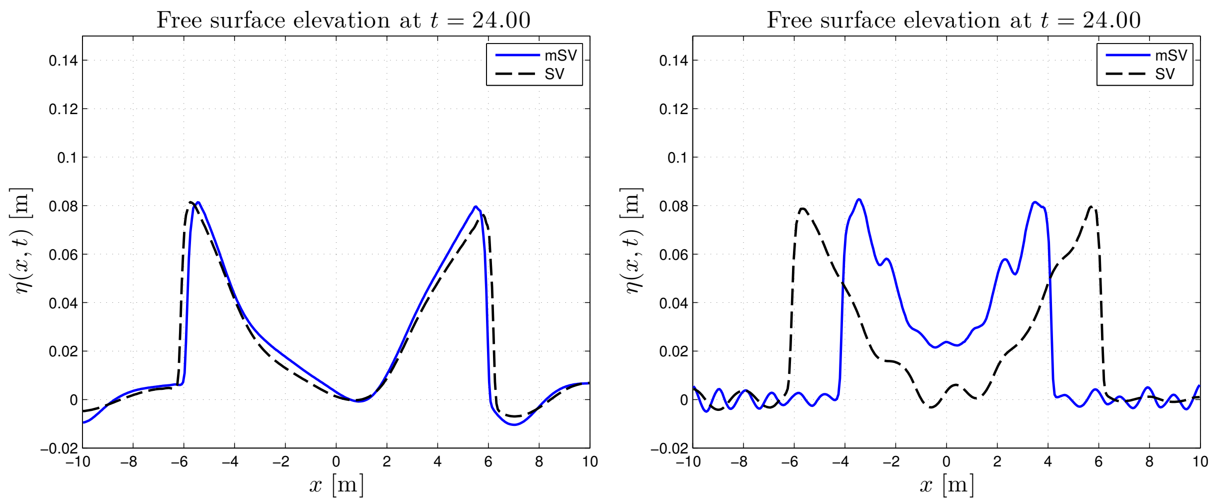

(a) Low oscillations (k_1) (b) High oscillations (k_2)

FIGURE 9. Wave propagation over an oscillatory bottom, $t = 24\ \mathsf{s}$.

First, we present numerical results (see Figures 11–12) corresponding to a relatively slow uplift of a portion of the bottom ($\alpha_1 = 2.0$). There is a very good agreement between two computations. We note that the amplitude of bottom deformation $a/d = 0.25$ is strong which explains some small discrepancies on Figure 12(a) between two models. This effect is rather due to the bottom shape than to its dynamic motion.

Then we test the same situation but the bottom uplift is fast with the inverse characteristic time $\alpha_2 = 12.0$. In this case the differences between two models are very flagrant. As it can be seen on Figure 14, for example, the modified Saint-Venant equations give a wave

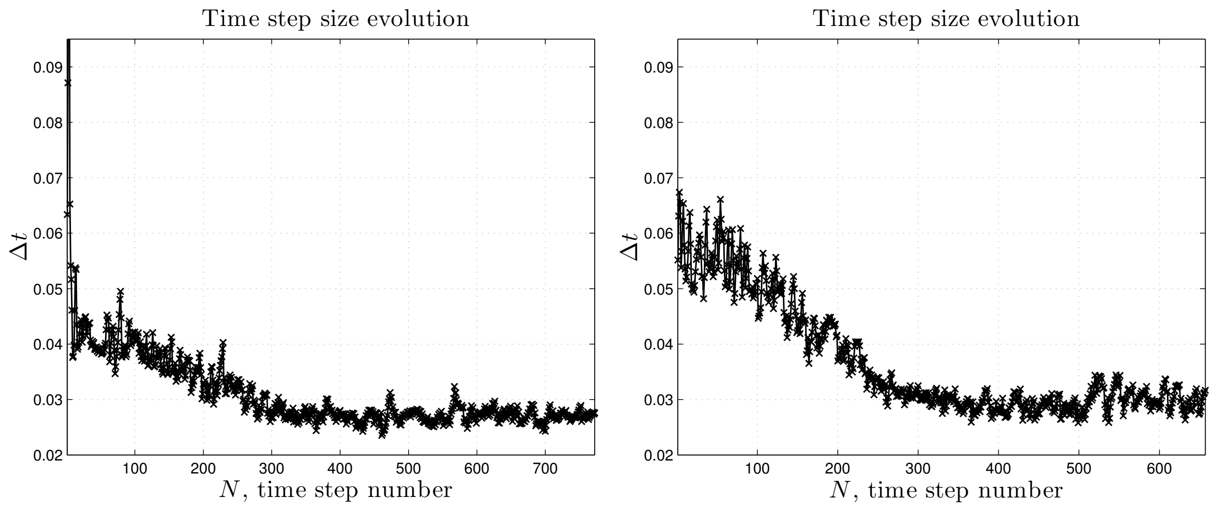

(a) Low oscillations (k_1) (b) High oscillations (k_2)

FIGURE 10. Local time step size during the simulation of a wave propagation over an oscillatory bottom test case.

Slow uplift parameter α_1:	$2.0\,\mathrm{s}^{-1}$
Fast uplift parameter α_2:	$12.0\,\mathrm{s}^{-1}$
Gravity acceleration g:	$1\,\mathrm{m\,s}^{-2}$
Final simulation time T:	$5\,\mathrm{s}$
Undisturbed water depth d_0:	$1\,\mathrm{m}$
Deformation amplitude a:	$0.25\,\mathrm{m}$
Half-length of the uplift area b:	$2.5\,\mathrm{m}$

TABLE 3. Values of various parameters used for the wave generation by a moving bottom.

with almost two times higher amplitude. Some differences in the wave shape persist even during the propagation (see Figure 16). This test-case clearly shows another advantage of the modified Saint-Venant equations in better representation of the vertical velocity field.

On Figure 17 we show the evolution of the local time step adapted while solving the modified Saint-Venant equations with moving bottom (up to $T = 5\,\mathrm{s}$). We can observe a behaviour very similar to the result presented above (see Figure 10) for the wave propagation test-case.

4.3. **Application to tsunami waves.** Tsunami waves continue to pose various difficult problems to scientists, engineers and local authorities. There is one question initially stemming from the Ph.D. thesis of C. SYNOLAKIS [74]. On page 85 of his manuscript, one can find a comparison between a theoretical (NSWE) and an experimental wavefront paths during a solitary wave runup onto a plane beach. In particular, his results show some

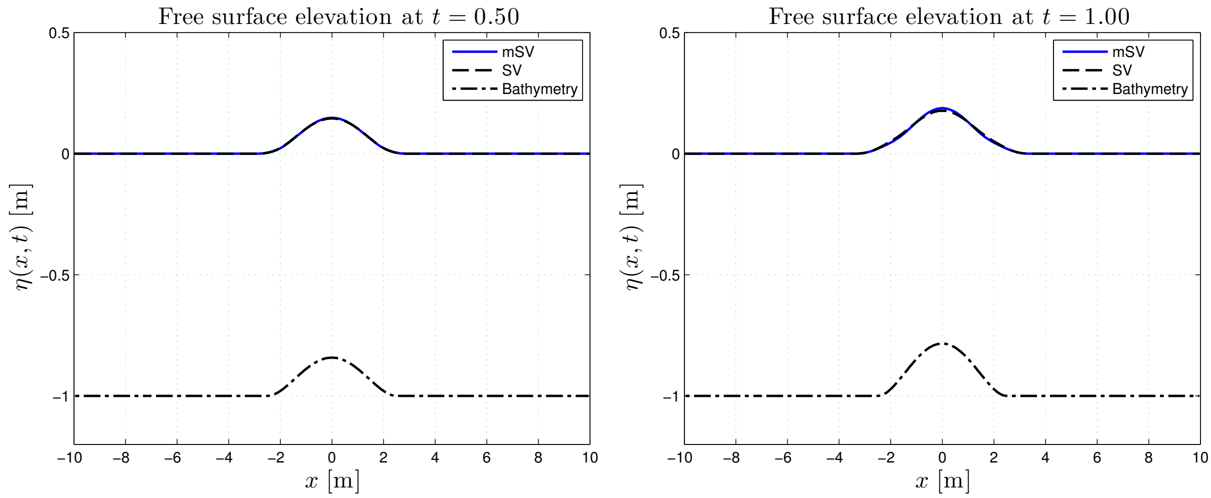

(a) $t = 0.5\,\mathrm{s}$ (b) $t = 1.0\,\mathrm{s}$

FIGURE 11. Slow bottom uplift test-case ($\alpha_1 = 2$).

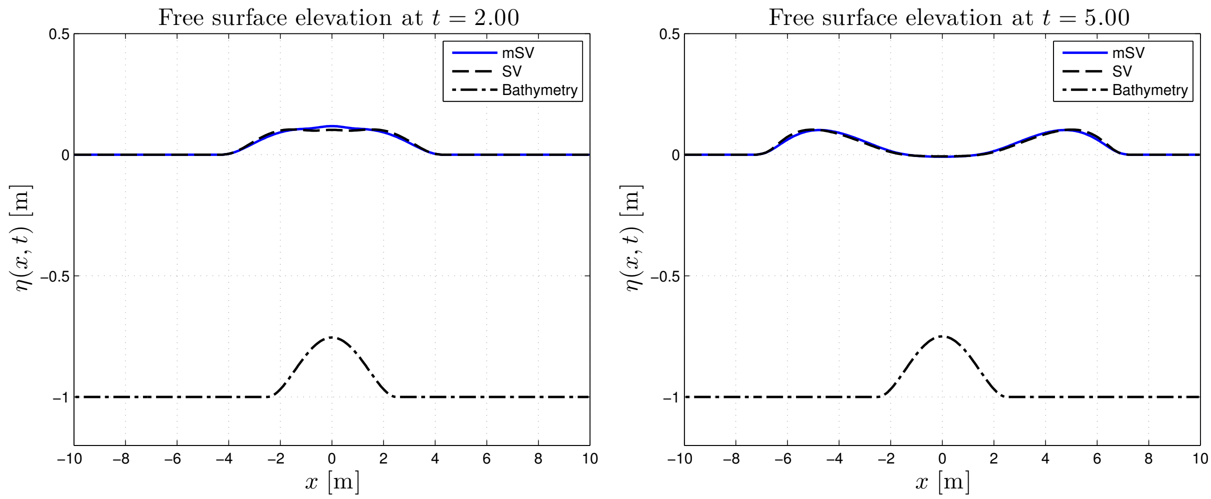

(a) $t = 2.0\,\mathrm{s}$ (b) $t = 5.0\,\mathrm{s}$

FIGURE 12. Slow bottom uplift test-case ($\alpha_1 = 2$).

discrepancy whose importance was not completely recognized until the wide availability of videos of the Tsunami Boxing Day 2004 [3, 59, 77]. In the same line of thinking, we quote here a recent review by SYNOLAKIS & BERNARD (2006) [76] which contains a very interesting paragraph:

> *"In a video taken near the Grand Mosque in Aceh, one can infer that the wavefront first moved at speeds less than 8 km h^{-1}, then accelerated to 35 km h^{-1}. The same phenomenon is probably responsible for the mesmerization of victims during tsunami attacks, first noted in series of photographs*

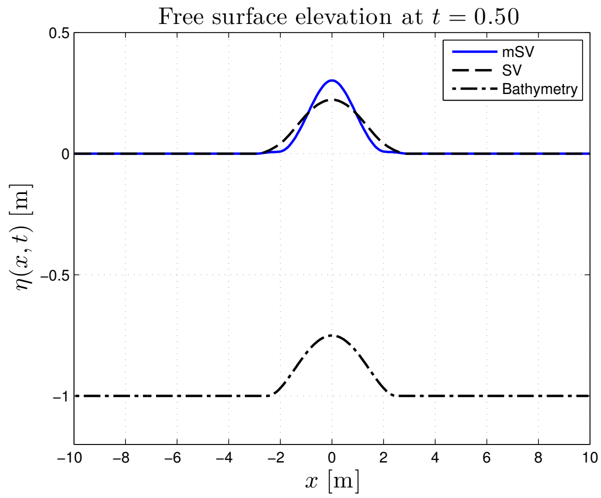

(a) $t = 0.5\,\mathsf{s}$

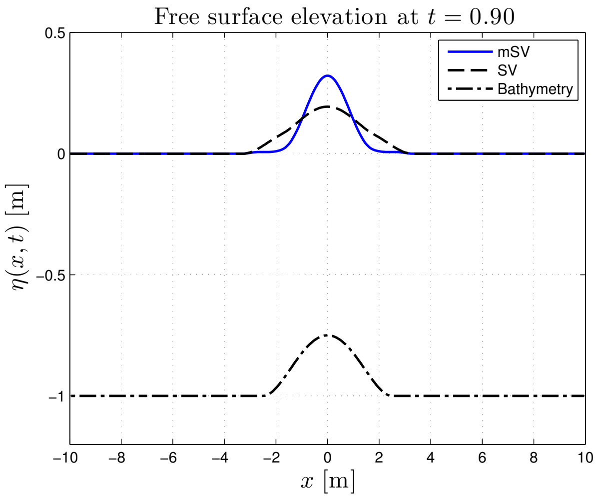

(b) $t = 0.9\,\mathsf{s}$

FIGURE 13. Fast bottom uplift test-case ($\alpha_2 = 12$).

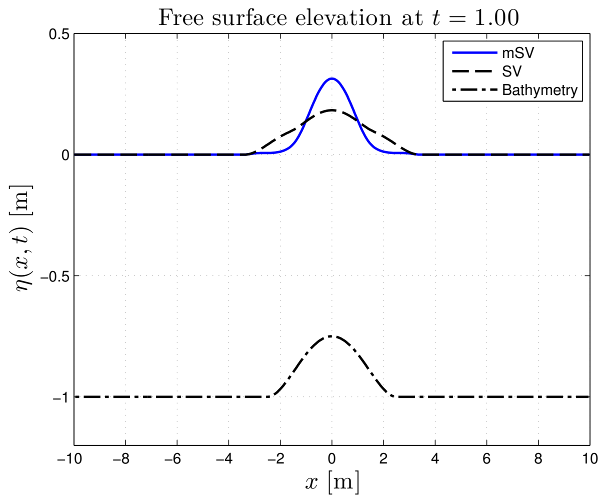

(a) $t = 1.0\,\mathsf{s}$

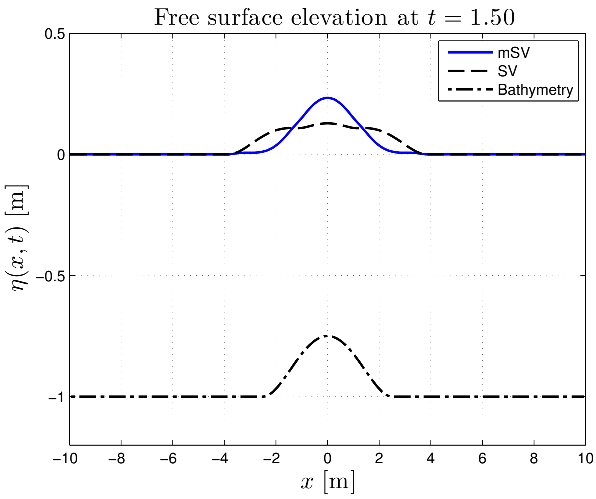

(b) $t = 1.5\,\mathsf{s}$

FIGURE 14. Fast bottom uplift test-case ($\alpha_2 = 12$).

> *of the 1946 Aleutian tsunami approaching Hilo, Hawaii, and noted again in countless photographs and videos from the 2004 megatsunami. The wavefront appears slow as it approaches the shoreline, leading to a sense of false security, it appears as if one can outrun it, but then the wavefront accelerates rapidly as the main disturbance arrives."*

Since our model is able to take into account the local bottom roughness into the wave speed computation, we propose below a simple numerical setup which intends to shed some

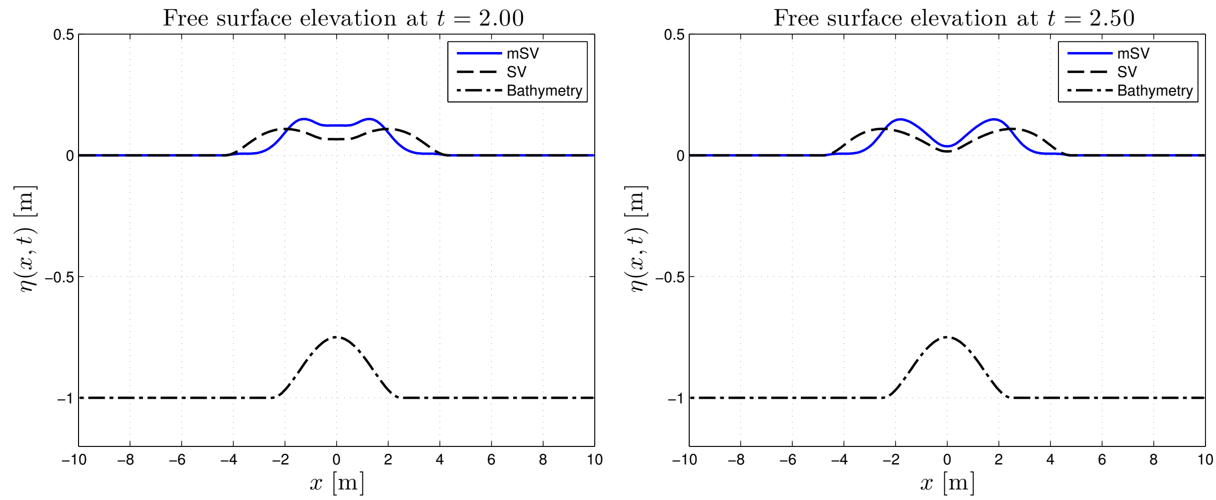

(a) $t = 2.0$ s (b) $t = 2.5$ s

FIGURE 15. Fast bottom uplift test-case ($\alpha_2 = 12$).

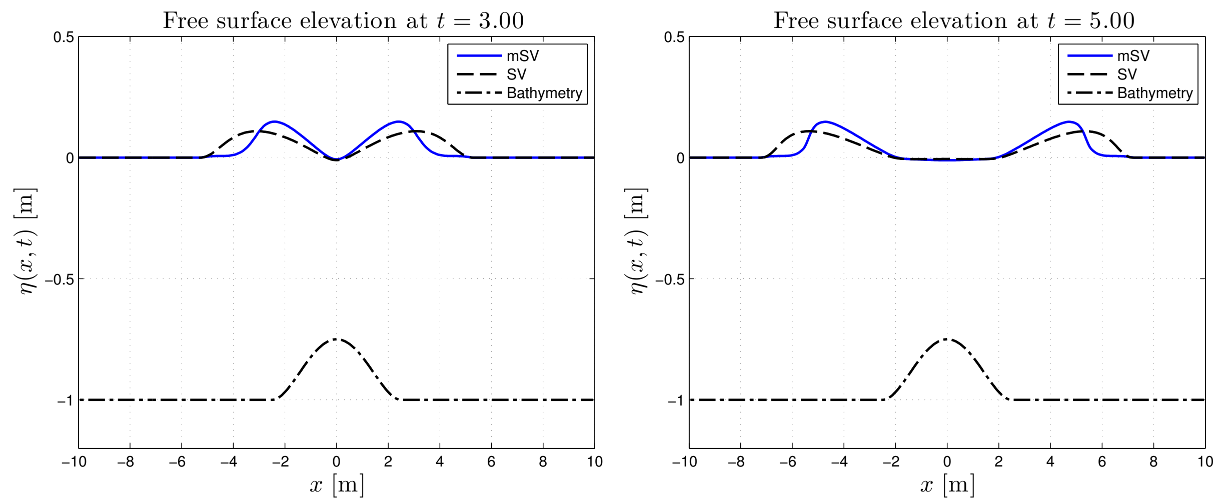

(a) $t = 3.0$ s (b) $t = 5.0$ s

FIGURE 16. Fast bottom uplift test-case ($\alpha_2 = 12$).

light on possible mechanism of the the reported hereinabove wave front propagation anomalies. Consider a one-dimensional domain $[-20, 20]$ with wall boundary conditions. This domain is discretised into $N = 4000$ control volumes in order to resolve local bathymetry oscillations. The bottom has a uniform slope which is perturbed on the left side ($x < 0$) by fast oscillations which model the bottom roughness

$$d(x) \;=\; d_0 \;-\; x\tan(\delta) \;+\; a\,[\,1 - \mathrm{H}(x)\,]\sin(kx), \tag{4.1}$$

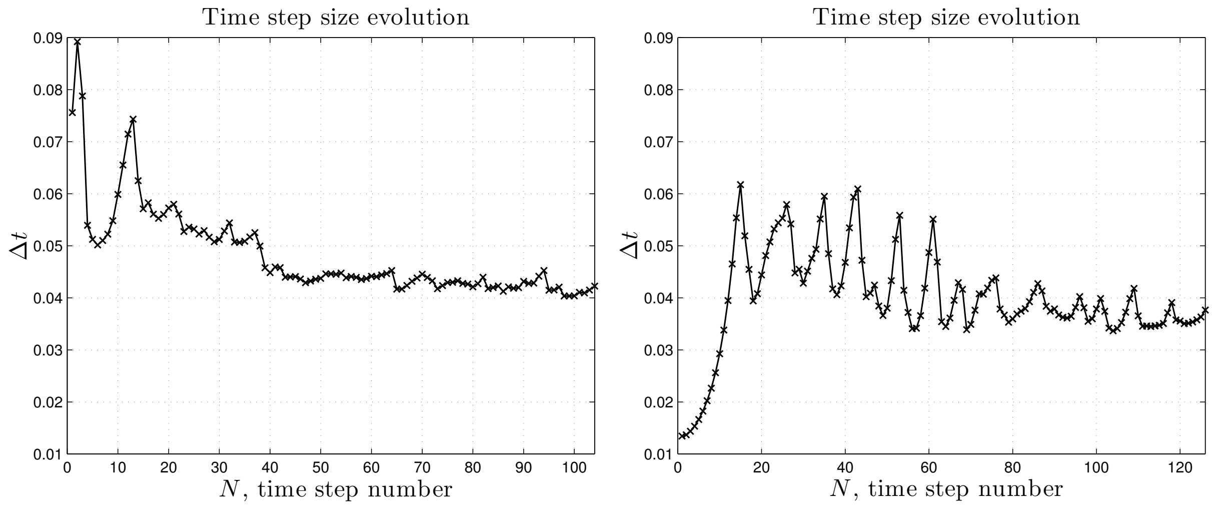

(a) Slow uplift (α_1) (b) Fast uplift (α_2)

FIGURE 17. Local time step size evolution during the simulation of a wave generation by moving bottom.

Undisturbed water depth d_0:	$1\,\mathrm{m}$
Gravity acceleration g:	$1\,\mathrm{m\,s^{-2}}$
Bottom slope $\tan(\delta)$:	0.02
Oscillation amplitude a:	$0.1\,\mathrm{m}$
Oscillation wavenumber k:	$20\,\mathrm{m^{-1}}$
Final simulation time T:	$19\,\mathrm{s}$
Solitary wave amplitude A:	$0.3\,\mathrm{m}$
Solitary wave initial position x_0:	$-12.0\,\mathrm{m}$

TABLE 4. Values of various physical parameters used for the wave propagation over a sloping bottom.

where $\mathrm{H}(x)$ is the Heaviside function. The initial condition is a solitary wave moving rightwards as it was chosen in [74, 75]:

$$\eta_0(x) \;=\; A\,\mathrm{sech}^2\!\left(\tfrac{1}{2}\kappa(x-x_0)\right), \qquad u_0(x) \;=\; \frac{c_0\,\eta_0(x)}{d(x_0)+\eta_0(x)},$$

$$\kappa \;=\; \sqrt{\frac{3\,A}{1+A}}, \qquad c_0 \;=\; \frac{\sqrt{6\,g}(1+A)}{\sqrt{3+2A}}\cdot\frac{\sqrt{(1+A)\log(1+A)-A}}{A}.$$

This configuration aims to model a wave transition from rough to gentle bottoms. The values of various physical parameters are given in Table 4.

Then, the wave propagation and transformation over the sloping bottom (4.1) was computed using the classical and modified Saint-Venant equations. The wave front position was measured along this simulation and the computation result is presented on Figure 18.

The slope of these curves represents physically the wave front propagation speed. Recall also that the point $x = 0$ corresponds to the transition between rough and gentle regions of the sloping beach.

As one can expect, the classical model does not really see the rough region except from tiny oscillations. An observer situated on the beach, looking at the upcoming wave modelled by classical Saint-Venant equations, will not see any change in the wave celerity. More precisely, the slope of the black dashed curve on Figure 18 is rather constant up to the graphical resolution. On the other hand, one can see a drastic change in the wave front propagation speed predicted by the modified Saint-Venant equations when the bottom roughness disappears.

The scenario we present in this section is only a first attempt to shed some light on the reported anomalies in tsunami waves arrival time on the beaches. For instance, a comprehensive study of P. Wessel (2009) [82] shows that the reported tsunami travel time is often exceeds slightly the values predicted by the classical shallow water theory (see, for example, Figures 5 and 6 in [82]). This fact supports indirectly our theory. Certainly this mechanism does not apply to laboratory experiments but it can be a good candidate to explain the wave front anomalies in natural environments. The mechanism we propose is only an element of explanation. Further investigations are needed to bring more validations to this approach.

We underline that the computational results rely on sound physical modelling without any ad-hoc phenomenological terms in the governing equations. Only an accurate bathymetry description is required to take the full advantage of the modified Saint-Venant equations.

5. Conclusions

In this study we derived a novel non-hydrostatic non-dispersive model of shallow water type which takes into account large bathymetric variations. Previously some attempt was already made in the literature to derive shallow water systems for arbitrary slopes and curvature [22, 11, 49]. However, our study contains a certain number of new elements with respect to the existing state of the art. Namely, our derivation procedure relies on a generalized Lagrangian principle of the water wave problem [16]. Moreover, we do not introduce any small parameter and our approximation is made through the choice of a suitable constrained ansatz. Resulting governing equations have a simple form and physically sound structure. Another new element is the introduction of arbitrary bottom time variations.

The proposed model is discretized with a finite volume scheme with adaptive time stepping to capture the underlying complex dynamics. The performance of this scheme is then illustrated on several test cases. Some implications to tsunami wave modeling are also suggested at the end of this study.

Among various perspectives we would like to underline the importance of a robust runup algorithm development using the current model. This research should shift forward the

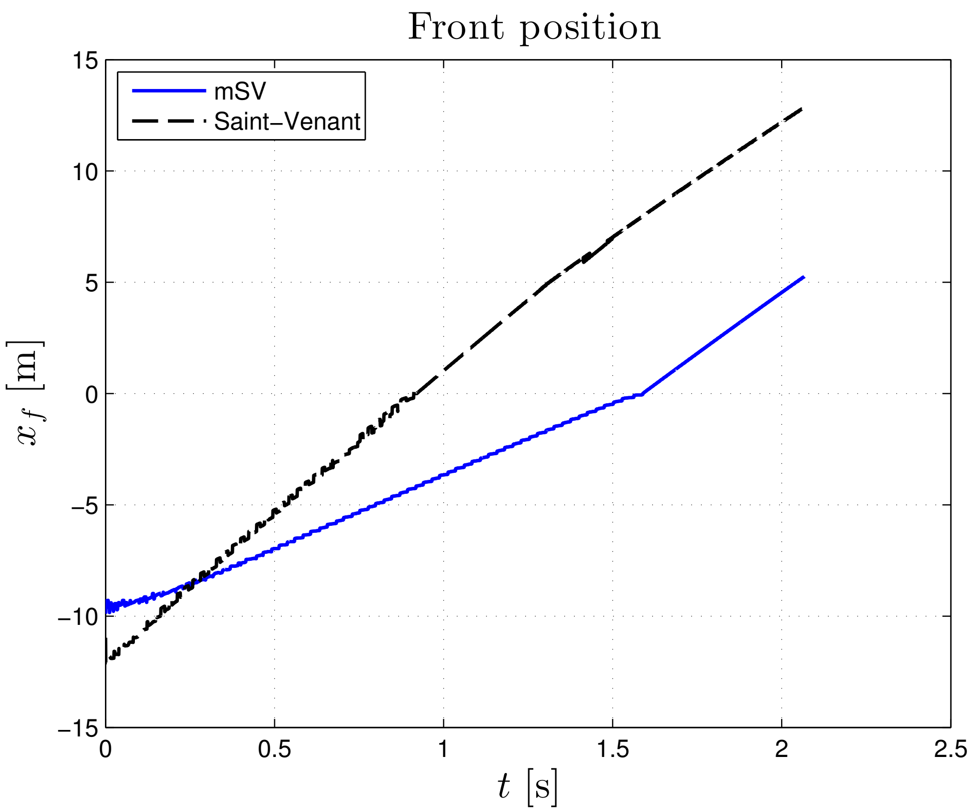

FIGURE 18. Wave front position computed with modified and classical Saint-Venant equations.

accuracy and our comprehension of a water wave runup onto complex shores [62, 36, 37, 30, 71, 33].

ACKNOWLEDGEMENTS

D. DUTYKH acknowledges the support from French Agence Nationale de la Recherche, project MathOcéan (Grant ANR-08-BLAN-0301-01).

We would like to thank Professor Valeriy LIAPIDEVSKII, Dimitrios MITSOTAKIS and Theodoros KATSAOUNIS for interesting discussions on gravity driven currents and finite volume schemes. We also thank Professor Thierry GALLOUËT for the suggestion to take into consideration steady solutions.

REFERENCES

[1] M. Abramowitz and I. A. Stegun. *Handbook of Mathematical Functions*. Dover, 1965. 8, 17

[2] F. Alcrudo and P. Garcia-Navarro. A high-resolution Godunov-type scheme in finite volumes for the 2D shallow-water equations. *Int. J. Numer. Methods Fluids*, 16(6):489–505, 1993. 2

[3] C. J. Ammon, C. Ji, H.-K. Thio, D. Robinson, S. Ni, V. Hjorleifsdottir, H. Kanamori, T. Lay, S. Das, D. Helmberger, G. Ichinose, J. Polet, and D. Wald. Rupture process of the 2004 Sumatra-Andaman earthquake. *Science*, 308:1133–1139, 2005. 21

[4] C. Ancey, V. Bain, E. Bardou, G. Borrel, R. Burnet, F. Jarry, O. Kolbl, and M. Meunier. *Dynamique des avalanches*. Presses polytechniques et universitaires romandes (Lausanne, Suisse), 2006. 2

[5] M. Antuono, V. Liapidevskii, and M. Brocchini. Dispersive Nonlinear Shallow-Water Equations. *Studies in Applied Mathematics*, 122(1):1–28, 2009. 2

[6] W. Artiles and A. Nachbin. Nonlinear evolution of surface gravity waves over highly variable depth. *Phys. Rev. Lett.*, 93(23):234501, 2004. 2

[7] T. J. Barth. Aspects of unstructured grids and finite-volume solvers for the Euler and Navier-Stokes equations. *Lecture series - van Karman Institute for Fluid Dynamics*, 5:1–140, 1994. 13

[8] T. J. Barth and M. Ohlberger. *Encyclopedia of Computational Mechanics, Volume 1, Fundamentals*, chapter Finite Vol. John Wiley and Sons, Ltd, 2004. 12, 13

[9] G. Bellotti and M. Brocchini. On using Boussinesq-type equations near the soreline: a note of caution. *Ocean Engineering*, 29:1569–1575, 2002. 2

[10] P. Bogacki and L. F. Shampine. A 3(2) pair of Runge-Kutta formulas. *Applied Mathematics Letters*, 2(4):321–325, 1989. 13

[11] F. Bouchut, A. Mangeney-Castelnau, B. Perthame, and J.-P. Vilotte. A new model of Saint-Venant and Savage-Hutter type for gravity driven shallow water flows. *C. R. Acad. Sci. Paris I*, 336:531–536, 2003. 2, 25

[12] L. J. F. Broer. On the Hamiltonian theory of surface waves. *Applied Sci. Res.*, 29(6):430–446, 1974. 3

[13] F. Chazel. Influence of bottom topography on long water waves. *M2AN*, 41:771–799, 2007. 2

[14] F. Chazel, D. Lannes, and F. Marche. Numerical simulation of strongly nonlinear and dispersive waves using a Green-Naghdi model. *J. Sci. Comput.*, 48:105–116, 2011. 2

[15] V. T. Chow. *Open-Channel Hydraulics*. Mcgraw-Hill College, 1959. 2

[16] D. Clamond and D. Dutykh. Practical use of variational principles for modeling water waves. *Physica D: Nonlinear Phenomena*, 241(1):25–36, 2012. 2, 4, 25

[17] A. J. C. de Saint-Venant. Théorie du mouvement non-permanent des eaux, avec application aux crues des rivières et à l'introduction des marées dans leur lit. *C. R. Acad. Sc. Paris*, 73:147–154, 1871. 2, 5

[18] A. Degasperis and M. Procesi. *Symmetry and Perturbation Theory*, chapter Asymptotic, pages 23–37. World Scientific, 1999. 2

[19] A. I. Delis and Th. Katsaounis. Relaxation schemes for the shallow water equations. *Int. J. Numer. Meth. Fluids*, 41:695–719, 2003. 5

[20] F. Dias and P. Milewski. On the fully-nonlinear shallow-water generalized Serre equations. *Physics Letters A*, 374(8):1049–1053, 2010. 2

[21] V. A. Dougalis and D. E. Mitsotakis. Theory and numerical analysis of Boussinesq systems: A review. In N A Kampanis, V A Dougalis, and J A Ekaterinaris, editors, *Effective Computational Methods in Wave Propagation*, pages 63–110. CRC Press, 2008. 2

[22] R. F. Dressler. New nonlinear shallow-flow equations with curvature. *Journal of Hydraulic Research*, 16(3):205–222, 1978. 2, 25

[23] D. Dutykh. *Mathematical modelling of tsunami waves*. Ph.d. thesis, École Normale Supérieure de Cachan, December 2007. 16, 18

[24] D. Dutykh. *Mathematical modeling in the environment*. Habilitation à diriger des recherches, Université de Savoie, December 2010. 16

[25] D. Dutykh and D. Clamond. Shallow water equations for large bathymetry variations. *J. Phys. A: Math. Theor.*, 44(33):332001, 2011. 2

[26] D. Dutykh and F. Dias. Dissipative Boussinesq equations. *C. R. Mecanique*, 335:559–583, 2007. 2

[27] D. Dutykh and F. Dias. Water waves generated by a moving bottom. In Anjan Kundu, editor, *Tsunami and Nonlinear waves*, pages 65–96. Springer Verlag (Geo Sc.), 2007. 16, 18

[28] D. Dutykh and F. Dias. Energy of tsunami waves generated by bottom motion. *Proc. R. Soc. A*, 465:725–744, 2009. 10

[29] D. Dutykh, F. Dias, and Y. Kervella. Linear theory of wave generation by a moving bottom. *C. R. Acad. Sci. Paris, Ser. I*, 343:499–504, 2006. 16

[30] D. Dutykh, T. Katsaounis, and D. Mitsotakis. Dispersive wave runup on non-uniform shores. In J. et al. Fort, editor, *Finite Volumes for Complex Applications VI - Problems & Perspectives*, pages 389–397, Prague, 2011. Springer Berlin Heidelberg. 2, 26

[31] D. Dutykh, Th. Katsaounis, and D. Mitsotakis. Finite volume methods for unidirectional dispersive wave models. *Submitted*, 2010. 15

[32] D. Dutykh, Th. Katsaounis, and D. Mitsotakis. Finite volume schemes for dispersive wave propagation and runup. *J. Comput. Phys*, 230:3035–3061, 2011. 2, 12, 13, 15

[33] D. Dutykh, C. Labart, and D. Mitsotakis. Long wave run-up on random beaches. *Phys. Rev. Lett*, 107:184504, 2011. 2, 26

[34] D. Dutykh and D. Mitsotakis. On the relevance of the dam break problem in the context of nonlinear shallow water equations. *Discrete and Continuous Dynamical Systems - Series B*, 13(4):799–818, 2010. 2, 5

[35] D. Dutykh, R. Poncet, and F. Dias. The VOLNA code for the numerical modeling of tsunami waves: Generation, propagation and inundation. *Eur. J. Mech. B/Fluids*, 30(6):598–615, 2011. 2

[36] H. M. Fritz, W. Kongko, A. Moore, B. McAdoo, J. Goff, C. Harbitz, B. Uslu, N. Kalligeris, D. Suteja, K. Kalsum, V. V. Titov, A. Gusman, H. Latief, E. Santoso, S. Sujoko, D. Djulkarnaen, H. Sunendar, and C. Synolakis. Extreme runup from the 17 July 2006 Java tsunami. *Geophys. Res. Lett.*, 34:L12602, 2007. 26

[37] D. R. Fuhrman and P. A. Madsen. Tsunami generation, propagation, and run-up with a high-order Boussinesq model. *Coastal Engineering*, 56(7):747–758, 2009. 26

[38] D. L. George. Augmented Riemann solvers for the shallow water equations over variable topography with steady states and inundation. *J. Comput. Phys.*, 227:3089–3113, 2008. 2

[39] J.-M. Ghidaglia, A. Kumbaro, and G. Le Coq. Une méthode volumes-finis à flux caractéristiques pour la résolution numérique des systèmes hyperboliques de lois de conservation. *C. R. Acad. Sci. I*, 322:981–988, 1996. 12

[40] J.-M. Ghidaglia, A. Kumbaro, and G. Le Coq. On the numerical solution to two fluid models via cell centered finite volume method. *Eur. J. Mech. B/Fluids*, 20:841–867, 2001. 12

[41] J.M.N.T. Gray, M Wieland, and K Hutter. Gravity-driven free surface flow of granular avalanches over complex basal topography. *Proc. R. Soc. Lond. A*, 455:1841–1874, 1998. 2

[42] A. E. Green and P. M. Naghdi. A derivation of equations for wave propagation in water of variable depth. *J. Fluid Mech.*, 78:237–246, 1976. 2

[43] J. Hammack. A note on tsunamis: their generation and propagation in an ocean of uniform depth. *J. Fluid Mech.*, 60:769–799, 1973. 16, 18

[44] J. L. Hammack. *Tsunamis - A Model of Their Generation and Propagation*. PhD thesis, California Institute of Technology, 1972. 18

[45] A. Harten. ENO schemes with subcell resolution. *J. Comput. Phys*, 83:148–184, 1989. 12

[46] A. Harten and S. Osher. Uniformly high-order accurate nonscillatory schemes, I. *SIAM J. Numer. Anal.*, 24:279–309, 1987. 12, 13

[47] K. Hutter, Y. Wang, and S. P. Pudasaini. The Savage-Hutter avalanche model. How far can it be pushed? *Phil. Trans. R. Soc. Lond. A*, 363:1507–1528, 2005. 2

[48] R. S. Johnson. *A Modern Introduction to the Mathematical Theory of Water Waves*. Cambridge University Press, 2004. 3

[49] J. B. Keller. Shallow-water theory for arbitrary slopes of the bottom. *J. Fluid Mech*, 489:345–348, 2003. 2, 25

[50] Y. Kervella, D. Dutykh, and F. Dias. Comparison between three-dimensional linear and nonlinear tsunami generation models. *Theor. Comput. Fluid Dyn.*, 21:245–269, 2007. 16, 18

[51] N. E. Kolgan. Finite-difference schemes for computation of three dimensional solutions of gas dynamics and calculation of a flow over a body under an angle of attack. *Uchenye Zapiski TsaGI [Sci. Notes Central Inst. Aerodyn]*, 6(2):1–6, 1975. 12
[52] H. Lamb. *Hydrodynamics*. Cambridge University Press, 1932. 3
[53] J. C. Luke. A variational principle for a fluid with a free surface. *J. Fluid Mech.*, 27:375–397, 1967. 3
[54] P. A. Madsen, H. B. Bingham, and H. A. Schaffer. Boussinesq-type formulations for fully nonlinear and extremely dispersive water waves: derivation and analysis. *Proc. R. Soc. Lond. A*, 459:1075–1104, 2003. 2
[55] C. C. Mei. *The applied dynamics of ocean surface waves*. World Scientific, 1994. 3
[56] J. W. Miles and R. Salmon. Weakly dispersive nonlinear gravity waves. *J. Fluid Mech.*, 157:519–531, 1985. 2
[57] D. E. Mitsotakis. Boussinesq systems in two space dimensions over a variable bottom for the generation and propagation of tsunami waves. *Math. Comp. Simul.*, 80:860–873, 2009. 2, 16
[58] A. Nachbin. A terrain-following Boussinesq system. *SIAM Appl. Math.*, 63(3):905–922, 2003. 2
[59] S. Neetu, I. Suresh, R. Shankar, D. Shankar, S. S. C. Shenoi, S. R. Shetye, D. Sundar, and B. Nagarajan. Comment on "The Great Sumatra-Andaman Earthquake of 26 December 2004". *Science*, 310:1431a–1431b, 2005. 21
[60] O. Nwogu. Alternative form of Boussinesq equations for nearshore wave propagation. *J. Waterway, Port, Coastal and Ocean Engineering*, 119:618–638, 1993. 2
[61] J. Pedlosky. *Geophysical Fluid Dynamics*. Springer, 1990. 2
[62] E. N. Pelinovsky and R. Kh. Mazova. Exact analytical solutions of nonlinear problems of tsunami wave run-up on slopes with different profiles. *Nat. Hazards*, 6(3):227–249, 1992. 26
[63] D. H. Peregrine. Long waves on a beach. *J. Fluid Mech.*, 27:815–827, 1967. 2
[64] A. A. Petrov. Variational statement of the problem of liquid motion in a container of finite dimensions. *Prikl. Math. Mekh.*, 28(4):917–922, 1964. 3
[65] R. Poncet and F. Dias. On the inclusion of arbitrary topography and bathymetry in the nonlinear shallow-water equations. In *XXII ICTAM, 25 - 29 August 2008, Adelaide, Australia*, 2008. 5
[66] S. B. Savage and K. Hutter. The motion of a finite mass of granular material down a rough incline. *J. Fluid Mech.*, 199:177—-215, 1989. 2
[67] F. Serre. Contribution à l'étude des écoulements permanents et variables dans les canaux. *La Houille blanche*, 8:374–872, 1953. 2
[68] L. F. Shampine and M. W. Reichelt. The MATLAB ODE Suite. *SIAM Journal on Scientific Computing*, 18:1–22, 1997. 14
[69] G. Söderlind. Digital filters in adaptive time-stepping. *ACM Trans. Math. Software*, 29:1–26, 2003. 14
[70] G. Söderlind and L. Wang. Adaptive time-stepping and computational stability. *Journal of Computational and Applied Mathematics*, 185(2):225–243, 2006. 14
[71] T. Stefanakis, F. Dias, and D. Dutykh. Local Runup Amplification by Resonant Wave Interactions. *Phys. Rev. Lett.*, 107:124502, 2011. 26
[72] J. J. Stoker. *Water Waves: The mathematical theory with applications*. Interscience, New York, 1957. 2, 5
[73] J. J. Stoker. *Water waves, the mathematical theory with applications*. Wiley, 1958. 3, 10
[74] C. Synolakis. *The runup of long waves*. PhD thesis, California Institute of Technology, 1986. 20, 24
[75] C. Synolakis. The runup of solitary waves. *J. Fluid Mech.*, 185:523–545, 1987. 2, 24
[76] C. E. Synolakis and E. N. Bernard. Tsunami science before and beyond Boxing Day 2004. *Phil. Trans. R. Soc. A*, 364:2231–2265, 2006. 21
[77] V. V. Titov, A. B. Rabinovich, H. O. Mofjeld, R. E. Thomson, and F. I. González. The global reach of the 26 December 2004 Sumatra tsunami. *Science*, 309:2045–2048, 2005. 21
[78] M. I. Todorovska and M. D. Trifunac. Generation of tsunamis by a slowly spreading uplift of the seafloor. *Soil Dynamics and Earthquake Engineering*, 21:151–167, 2001. 16

[79] B. van Leer. Towards the ultimate conservative difference scheme V: a second order sequel to Godunov' method. *J. Comput. Phys.*, 32:101–136, 1979. 12
[80] B. van Leer. Upwind and High-Resolution Methods for Compressible Flow: From Donor Cell to Residual-Distribution Schemes. *Communications in Computational Physics*, 1:192–206, 2006. 12
[81] G. Wei, J. T. Kirby, S. T. Grilli, and R. Subramanya. A fully nonlinear Boussinesq model for surface waves. Part 1. Highly nonlinear unsteady waves. *J. Fluid Mech.*, 294:71–92, 1995. 2
[82] P. Wessel. Analysis of Observed and Predicted Tsunami Travel Times for the Pacific and Indian Oceans. *Pure Appl. Geophys.*, 166(1-2):301–324, February 2009. 25
[83] G. B. Whitham. A general approach to linear and non-linear dispersive waves using a Lagrangian. *J. Fluid Mech.*, 22:273–283, 1965. 3
[84] G. B. Whitham. *Linear and nonlinear waves.* John Wiley & Sons Inc., New York, 1999. 3
[85] Y. Xing and C.-W. Shu. High order finite difference WENO schemes with the exact conservation property for the shallow water equations. *J. Comput. Phys.*, 208:206–227, 2005. 12
[86] N. Zahibo, E. Pelinovsky, T. Talipova, and N. Nikolkina. Savage-Hutter model for avalanche dynamics in inclined channels: analytical solutions. *Journal of Geophysical Research*, 115:B03402, 2010. 2
[87] V. E. Zakharov. Stability of periodic waves of finite amplitude on the surface of a deep fluid. *J. Appl. Mech. Tech. Phys.*, 9:1990–1994, 1968. 3
[88] J. G. Zhou, D. M. Causon, D. M. Ingram, and C. G. Mingham. Numerical solutions of the shallow water equations with discontinuous bed topography. *Int. J. Numer. Meth. Fluids*, 38:769–788, 2002. 2

LAMA, UMR 5127 CNRS, Université de Savoie, Campus Scientifique, 73376 Le Bourget-du-Lac Cedex, France
E-mail address: `Denys.Dutykh@univ-savoie.fr`
URL: `http://www.lama.univ-savoie.fr/~dutykh/`

Laboratoire J.-A. Dieudonné, Université de Nice – Sophia Antipolis, Parc Valrose, 06108 Nice cedex 2, France
E-mail address: `diderc@unice.fr`
URL: `http://math.unice.fr/~didierc/`